A Fast Bayesian Inference Scheme for Recovering Mechanical Properties of Layered Composites based on Wave and Finite Element-assisted Metamodeling Strategy

Wang-Ji Yan[1], Dimitrios Chronopoulos[2], Sergio Cantero-Chinchilla[2,3], Ka-Veng Yuen[1], Costas Papadimitriou[4]

[1]State Key Laboratory of Internet of Things for Smart City and Department of Civil and Environmental Engineering, University of Macau, People's Republic of China
[2]Institute for Aerospace Technology & The Composites Group, The University of Nottingham, United Kingdom
[3]Aernnova Engineering Division S.A., Madrid 28034, Spain
[4]Department of Mechanical Engineering, University of Thessaly, Greece

Abstract: Reliable verification and evaluation of the mechanical properties of an assembled layered composite ensemble are critical for industrially relevant applications, but it still remains an open engineering challenge. In this study, a fast Bayesian inference scheme based on multi-frequency single shot measurements of wave propagation characteristics is developed to overcome the limitations of ill-conditioning and non-uniqueness associated with the conventional approaches. A Transitional Markov chain Monte Carlo (TMCMC) algorithm is employed for the sampling process. A Wave and Finite Element (WFE)-assisted metamodeling scheme in lieu of expensive-to-evaluate explicit FE analysis is proposed to cope with the high computational cost involved in TMCMC sampling. For this, the Kriging predictor providing a surrogate mapping between the probability spaces of the model predictions for the wave characteristics and the mechanical properties in the likelihood evaluations is established based on the training outputs computed using a WFE forward solver, coupling periodic structure theory to conventional FE. The valuable uncertainty information of the prediction variance introduced by the use of a surrogate model are also properly taken into account when estimating the parameters' posterior probability distribution by TMCMC. A numerical study as well as an experimental study are conducted to verify the computational efficiency and accuracy of the proposed methodology. Results show that the TMCMC algorithm in conjunction with the WFE forward solver-aided metamodeling can sample the posterior Probability Density Function (PDF) of the updated parameters at a very reasonable cost. This approach is capable of quantifying the uncertainties of recovered independent characteristics for each layer of the composite structure under investigation through fast and inexpensive experimental measurements on localized portions of the structure.

Key words: Ultrasonic guided waves; Wave and finite element; Bayesian analysis; Composite structure; Uncertainty quantification; Metamodel

Nomenclature:

x_0: the excitation location
x_1: the monitoring location
ω_k: the k-th frequency point of the wave characteristics
$y_{\omega_k}^{mea}$: the measurements of wave characteristics at frequency ω_k
L: the propagation distance of the wave
$H\left[x(t)\right]$: Hilbert Transform of $x(t)$
$\Delta t\big|_{\omega_k}$: the difference of time of flight for the excitation frequency ω_k
$\boldsymbol{\theta}$: the damage characterization parameters
$y_{\omega_k}^{model}(\boldsymbol{\theta})$: the wave characteristics predicted by $\boldsymbol{\theta}$ using WFEM scheme
$x(t)$: time history signal
$\mathbf{K}$, $\mathbf{C}$ and $\mathbf{M}$**:** the stiffness, viscous damping and mass matrices of the segment
$\mathbf{u}$: the displacement vector
$\mathbf{F}$: the forcing vector
$\mathbf{D}$: frequency dependent dynamic stiffness matrix
Q, R, S and T: subscripts denoting the periodic edges
λ_x and λ_y: the phase constants
κ_x and κ_y: the wavenumbers
$\mathbf{I}$: the identity matrix
$\boldsymbol{\Theta}$: vectors of independent input parameters
$\boldsymbol{\theta}^{(i)}$: i-th sample generated by using the DoE strategy
n_s: the number of DoE samples
n_p: the number of parameters to be identified
$\mathrm{G}_{\omega_k}(\boldsymbol{\Theta})$**:** a vector of training data outputs corresponding to $\boldsymbol{\Theta}$
$y_{\omega_k}^{model}\left(\boldsymbol{\theta}^{(i)}\right)$: the wave characteristics predicted at $\boldsymbol{\theta}^{(i)}$
$\eta_{\omega_k}(\boldsymbol{\theta})$: metamodel at ω_k
$f_{\omega_k}(\boldsymbol{\theta})$: a regression function constructed based on the data
$\vartheta_{\omega_k}(\boldsymbol{\theta})$: a Gaussian process constructed through the residuals
$\sigma_{\omega_k}^2$: the process variance
$\mathrm{Cov}\left(\vartheta_{\omega_k}(\Theta)\right)$: the covariance matrix of $\vartheta_{\omega_k}(\Theta)$
$\boldsymbol{Y}_{\omega_k}(\Theta)$: a parametric correlation function
$\varphi\left(\boldsymbol{\theta}^{(p)}, \boldsymbol{\theta}^{(q)}\right)$: the correlation function between training data $\boldsymbol{\theta}^{(p)}$ and $\boldsymbol{\theta}^{(q)}$
υ_j: hyper-parameters describing the influence sphere of a point on nearby points
$\mu_{\omega_k}\left(\boldsymbol{\theta}^*, \Theta\right)$: mean of the Kriging predictor
$\mathrm{S}_{\omega_k}\left(\boldsymbol{\theta}^*, \Theta\right)$: standard deviation of the Kriging predictor

$\eta_{\omega_k}\left(\boldsymbol{\theta}^*\right)$: the scattering coefficients predicted by Kriging model at $\boldsymbol{\theta}^*$

ϖ : all model parameters to be identified

$\mathcal{D}$: is the available data (i.e. the scattering property estimates)

M : the model class

$p\left(\mathcal{D}\middle|\mathrm{M},\varpi\right)$: the likelihood function of the data $\mathcal{D}$

$p\left(\varpi\middle|\mathrm{M}\right)$: the prior PDF of the parameters

$p\left(\varpi\middle|\mathrm{M},\mathcal{D}\right)$: the posterior PDF of the parameters

$p\left(\mathcal{D}\middle|\mathrm{M}\right)$: a normalization factor ensuring that the posterior PDF integrates to 1

$\chi_{\omega_k}\left(\boldsymbol{\theta}^*\right)$: a random variable with zero mean and variance $\mathrm{S}^2_{\omega_k}\left(\boldsymbol{\theta}^*\right)$

ε_{ω_k} : additional white noise representing the measurement noise and model error

σ_ε^2 : the variances of the prediction errors ε_{ω_k}

$\mathrm{L}\left(\varpi\right)$: the negative-log likelihood function

$\pi_i\left(\varpi\right)$: the target PDF at stage i

$\pi_{i+1}\left(\varpi\right)$: the target PDF at stage $i+1$

$p_j\left(\varpi\middle|\mathrm{M},\mathcal{D}\right)$: intermediate probability distribution

q_j : factor controlling the transition between adjacent probability distributions

n_{stage} : the total number of TMCMC stages

$\left\{\varpi_{j,k}, k=1,\cdots,N_j\right\}$: samples from $p_j\left(\varpi\middle|\mathrm{M},\mathcal{D}\right)$ at stage j

$\left\{\varpi_{j+1,k}, k=1,\cdots,N_{j+1}\right\}$: samples from $p_{j+1}\left(\varpi\middle|\mathrm{M},\mathcal{D}\right)$ at stage $j+1$

$w(\varpi_{j,k})$: the plausibility weights

$COV\left(w(\varpi_{j,k})\right)$: the coefficient of variation of the plausibility weights

tol : a prescribed tolerance

1 Introduction

Layered and complex structures are nowadays widely used within the aerospace, automotive, construction and energy sectors with a general increase tendency [1,2]. Therefore, the development of strict quality control and nondestructive evaluation procedures to ensure that the characteristics of the employed layers match the requirements has been a natural target in the field of composites [3]. The evaluation and verification of the characteristics for each layer of the assembled layered composite structure remains an open engineering challenge worth further exploration. Experimental testing is expected to play important roles in detecting the mechanical properties of composites, assessing system conditions and reconciling numerical predictions. In this context, inverse techniques ought to be used as important tools to extract the information about the behavior of a structure directly from experimental data [4].

Nowadays, wave propagation techniques are often employed for verification and health monitoring purposes. Guided Waves (GW) can propagate at a long distance in thin waveguides and are sensitive to structural properties as well as defects [5]. Fast and accurate identification of the operational properties of such structures through non-destructive evaluation approaches is a challenging task for the modern engineer due to the lack of robust modelling approaches. Therefore, the propagation of guided waves in composite structures has indeed been the subject of intense research in recent years. Traditional analytical methods such as the classical plate theory and Mindlin-Reissner plate theory typically employed for modelling wave propagation in monolayers can only capture the wave characteristics in the low frequency range for thick and discontinuous structures [1]. Semi-analytical methods such as the Semi-Analytical Finite Element (SAFE) have been developed later on to address this issue. While the SAFE method is very time efficient when investigating a material that is discontinuous in its thickness but continuous in the direction of propagation, it encounters severe limitations when it comes to materials that are periodic in the direction of propagation [6]. In contrast, FE based wave methods assume a full 3D displacement field and are therefore capable of capturing the entirety of wave motion types in the waveguide under investigation in a very accurate and efficient manner [7,8]. The FE based analysis of wave propagation within complex periodic structures was firstly presented in [9] based on Periodic Structure Theory (PST), which was extended to two-dimensional media in [10]. Recently, the Wave Finite Element (WFE) method [11-13] was introduced to facilitate the post-processing of the eigenproblem solutions and further improve the computational efficiency of the method. The WFE method for 2D structures was introduced in [14]. Ultrasound computations with the PST and the WFE have recently been exhibited in [15].

More recently, WFE scheme was used to identify the characteristics of each individual layer of a composite structure through experimental measurements on the entire structure [1]. The method can account for structures of arbitrary complexity. Excitations with both low and high frequency can be employed for inverting the structural problem. However, it is worth mentioning that there is a mismatch between the level of information in the detailed theoretical model of uncertain accuracy as well as the relatively sparse information in the incomplete set of noisy test data, which produces an ill-conditioned and often nonunique inverse problem [16]. As a result, the solution that simply minimizes the residual of the measurements and prediction may not exist or is highly unstable due to a small amount of inevitable measurement noise.

Beck and Katafygiotis gave an appropriate statistical framework [17] for properly handling the uncertainties due to ill-conditioning and non-uniqueness associated with the inverse problem, which has been widely considered a candidate for easing the ill-posedness of the problem [18-24]. In the campaign of structural identification, another advantage of Bayesian statistical framework is that uncertainties due to endogenous factors that has been widely accepted can be appropriately considered [25, 26]. The framework is not only to give more accurate results for identification but also to provide a quantitative assessment of this accuracy [27].

Bayesian statistics have been widely applied in GW-based inverse problems. A number of new damage detection approaches incorporating Bayesian system identification framework in tandem with various technologies such as the Spectral Finite Element (SFE) method as well as advanced signal processing techniques, etc. were proposed by Ng et al. [28-31]. Bayesian approaches were developed to identify the damage location and wave velocity based on the time-of-flight (ToF) of the scattered waves [32,33]. In [34], the Bayesian framework was proposed to detect and quantify multiple flaws in structures by using the Extended Finite Element Method (XFEM) as the forward solver. A Bayesian method was used to statistically characterize the uncertain parameters in an ultrasonic inspection system from limited signal measurements to enhance the confidence on the probability of detection curve [35]. The sparse Bayesian learning approach [36,37] and multilevel Bayesian approach [38] were also utilized to deal with uncertainty in the context of ultrasound-based damage identification. A new crack size quantification method was presented based on in-situ Lamb wave testing and Bayesian method in [39]. The authors of [40] proposed a Bayesian approach for investigating the effects of manufacturing variability on the wavenumber identification of beams with evenly attached resonators produced from Selective Laser Sintering. In [41], a new Bayesian inference approach was proposed for damage identification based on analytical probabilistic model of scattering coefficient estimators and ultrafast wave scattering simulation scheme.

The novelty of this study is that it aims at recovering the mechanical properties of the layered structure through the acquired propagating wave characteristics in a Bayesian inference framework. It allows quantifying the uncertainties associated with the recovered results of mechanical properties and avoiding ill-conditioning as well as non-uniqueness associated with the conventional approaches. In the procedure of Bayesian inference, the stochastic simulation approaches such as MCMC tools usually require running the forward solver repeatedly. The computational cost of stochastic simulation is proportional to the scale of the FE model, the frequency points of the propagating wave characteristics as well as the dimension of the identification parameter set, etc., which can eliminate the appropriateness of available approaches due to the expense of carrying out an exhaustive number of runs. Worse still, FE modelling, wave predictions using forward solvers, as well as stochastic simulations are usually implemented in different software and languages (MATLAB, ABAQUS, ANSYS, etc.), which means that interfacing between different environments is an additional challenge in Bayesian uncertainty quantification.

To address this critical issue, the WFE scheme coupling periodic structure theory to conventional FE, being several orders of magnitudes faster than explicit FE modelling, will be employed to predict the wave propagation characteristics as forward solver. In addition, a cheap and fast Kriging metamodel, which provides a surrogate mapping between the probability spaces of the model predictions for the wave characteristics and the parameters to be recovered, will be employed to approximate the training outputs computed using the WFE scheme as a function of model parameters. The uncertainty of wave characteristics predicted by the metamodel as well as the overall prediction error are also properly accommodated in the likelihood function of Bayesian inference. Numerical and experimental studies indicate that the Transitional Markov chain Monte Carlo (TMCMC) algorithm [42] in conjunction with the WFE-assisted Kriging model can estimate the posterior Probability Density Function (PDF) of the updated parameters efficiently. It should be stressed that the proposed methodology is completely baseline-free with the only information required being the number of layers comprising the composite structure.

The paper is organized as follows: In Section 2, the FE computational scheme for predicting wave propagation in multilayered structures is presented. The experimental protocol for extracting wave properties is also introduced in this section. A fast Bayesian inference scheme incorporating WFE-aided metamodeling is presented in Section 3 to effectively recover the structural and material characteristics for the structure under investigation. The procedure is verified by recovering the mechanical characteristics using numerical and experimental examples in Section 4. Conclusions are eventually drawn in Section 5.

2 Wave Properties Extractions

2.1 Wave characteristics computation through a WFEM Scheme

The composite structure under consideration comprises a number of layers which may be of arbitrary anisotropy. The identifiable properties include the thickness as well as the material characteristics of each individual layer. A robust wave model which is expressed in terms of the material characteristics to be recovered can provide a good understanding and also form the basis of a characterization process for a mechanical system. Given the forward wave model, system identification can be implemented by fitting it to that from experimental testing. The review presented in this section is heavily borrowed from [14].

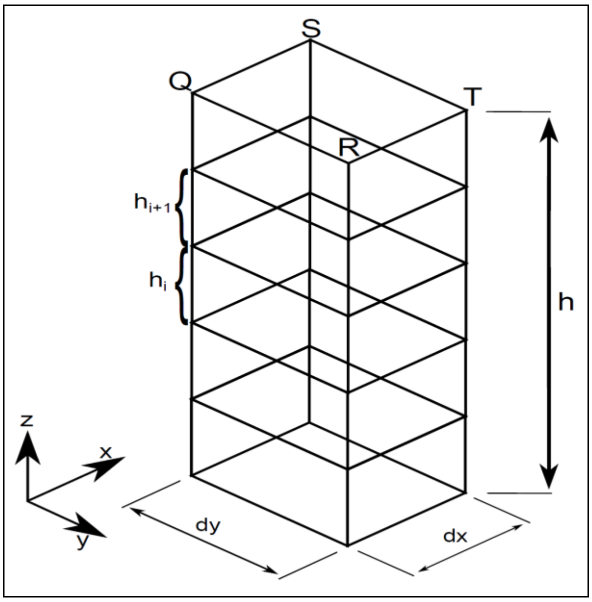

Fig. 1: Caption of the periodic segment of a composite panel of arbitrary layering modelled within the WFE scheme. Periodic edges are noted as Q, R, S and T.

It is stressed that the investigated case studies in this work are spatially continuous in the *x* and *y* directions. The WFE scheme can also deal with structures of fixed periodicity in a straightforward manner through condensation of the internal Degree of Freedom (DoF). For the periodic segment of a composite panel of arbitrary layering modelled within the WFE scheme shown in Fig. 1, the mass and stiffness and damping matrices of the periodic segment $\mathbf{M}$, $\mathbf{K}$ and $\mathbf{C}$ are extracted through standard FE modelling. Following the analysis presented in [14], the time-harmonic equation of motion of the segment assuming arbitrary damping can be written as:

$$\left(\mathbf{K} + \mathrm{i}\omega_k \mathbf{C} - \omega_k^2 \mathbf{M}\right)\mathbf{u} = \mathbf{F} \tag{1}$$

where $\mathbf{F}$ is the vector of the nodal forces. Then the dynamic stiffness matrix can be written as:

$$\mathbf{D} = \mathbf{K} + \mathrm{i}\omega_k \mathbf{C} - \omega_k^2 \mathbf{M} \tag{2}$$

The entries for each DoF, of every node laying on the same edge of the segment, say edges Q, R, S and T, are placed in the mass and stiffness matrices so that the vector of displacements can be written as: $\mathbf{u} = \{\mathbf{u}_Q; \mathbf{u}_R; \mathbf{u}_S; \mathbf{u}_T\}^{\mathrm{T}}$. Therefore, Eq.(1) may be written as:

$$\begin{bmatrix} \mathbf{D}_{QQ} & \mathbf{D}_{QR} & \mathbf{D}_{QS} & \mathbf{D}_{QT} \\ \mathbf{D}_{RQ} & \mathbf{D}_{RR} & \mathbf{D}_{RS} & \mathbf{D}_{RT} \\ \mathbf{D}_{SQ} & \mathbf{D}_{SR} & \mathbf{D}_{SS} & \mathbf{D}_{ST} \\ \mathbf{D}_{TQ} & \mathbf{D}_{TR} & \mathbf{D}_{TS} & \mathbf{D}_{TT} \end{bmatrix} \begin{Bmatrix} \mathbf{u}_Q \\ \mathbf{u}_R \\ \mathbf{u}_S \\ \mathbf{u}_T \end{Bmatrix} = \begin{Bmatrix} \mathbf{F}_Q \\ \mathbf{F}_R \\ \mathbf{F}_S \\ \mathbf{F}_T \end{Bmatrix} \tag{3}$$

Using the Floquet theory for a rectangular segment and assuming a time-harmonic response, the displacements of each edge can be written as a function of the displacements at a single edge. Taking edge Q as the edge of reference, we have:

$$\mathbf{u}_R = \lambda_x \mathbf{u}_Q \tag{4a}$$

$$\mathbf{u}_S = \lambda_y \mathbf{u}_Q \tag{4b}$$

$$\mathbf{u}_T = \lambda_x \lambda_y \mathbf{u}_Q \tag{4c}$$

with λ_x and λ_y the phase constants which are related to the wavenumbers κ_x and κ_y through the relation:

$$\lambda_x = e^{-\mathrm{i}\kappa_x d_x} \tag{5a}$$

$$\lambda_y = e^{-\mathrm{i}\kappa_y d_y} \tag{5b}$$

The displacement vector can therefore be written as:

$$\begin{Bmatrix} \mathbf{u}_Q \\ \mathbf{u}_R \\ \mathbf{u}_S \\ \mathbf{u}_T \end{Bmatrix} = \begin{Bmatrix} \mathbf{I} \\ \lambda_x \mathbf{I} \\ \lambda_y \mathbf{I} \\ \lambda_x \lambda_y \mathbf{I} \end{Bmatrix} \mathbf{u}_Q \tag{6}$$

Assuming no external excitation, equilibrium along edge Q implies that:

$$\{\mathbf{I} \quad \lambda_y^{-1}\mathbf{I} \quad \lambda_x^{-1}\mathbf{I} \quad \lambda_x^{-1}\lambda_y^{-1}\mathbf{I}\}\begin{Bmatrix}\mathbf{F}_Q\\\mathbf{F}_R\\\mathbf{F}_S\\\mathbf{F}_T\end{Bmatrix} = 0 \tag{7}$$

Eventually, substituting Eqs.(6) and (7) into Eq.(1), we end up with the eigenproblem:

$$\{\mathbf{I} \quad \lambda_y^{-1}\mathbf{I} \quad \lambda_x^{-1}\mathbf{I} \quad \lambda_x^{-1}\lambda_y^{-1}\mathbf{I}\}\mathbf{D}\begin{Bmatrix}\mathbf{I}\\\lambda_x\mathbf{I}\\\lambda_y\mathbf{I}\\\lambda_x\lambda_y\mathbf{I}\end{Bmatrix}\mathbf{u}_Q = 0 \tag{8}$$

which can be written in the form:

$$\begin{pmatrix}\left(\mathbf{D}_{QQ}+\mathbf{D}_{RR}+\mathbf{D}_{SS}+\mathbf{D}_{TT}\right)+\left(\mathbf{D}_{QR}+\mathbf{D}_{ST}\right)\lambda_x+\left(\mathbf{D}_{RQ}+\mathbf{D}_{TS}\right)\lambda_x^{-1}\\ +\left(\mathbf{D}_{QS}+\mathbf{D}_{RT}\right)\lambda_y+\left(\mathbf{D}_{SQ}+\mathbf{D}_{TR}\right)\lambda_y^{-1}+\mathbf{D}_{QT}\lambda_x\lambda_y+\\ \mathbf{D}_{TQ}\lambda_x^{-1}\lambda_y^{-1}+\mathbf{D}_{SR}\lambda_x\lambda_y^{-1}+\mathbf{D}_{RS}\lambda_x^{-1}\lambda_y\end{pmatrix}\mathbf{u}_Q = 0 \tag{9}$$

Various methods exist for the solution of the eigenproblem. In this work the scenario in which the frequency and the wavenumber towards y direction are considered as fixed will be adopted. For each set of fixed ω_k, κ_y the entirety of κ_x values are sought and values for intermediate ω_k, κ_x and κ_y can be found by interpolating on the known results. For a set of fixed ω_k, the non-linear eigenvalue problem of Eq.(9) is reduced to:

$$\left(\mathbf{A}_2\lambda_x^2+\mathbf{A}_1\lambda_x+\mathbf{A}_0\right)\mathbf{u}_Q = 0 \tag{10}$$

where

$$\mathbf{A}_j = \begin{cases}\mathbf{D}_{QT}\lambda_y^2+\left(\mathbf{D}_{QR}+\mathbf{D}_{ST}\right)\lambda_y+\mathbf{D}_{SR}, & j=2\\ \left(\mathbf{D}_{QQ}+\mathbf{D}_{RR}+\mathbf{D}_{SS}+\mathbf{D}_{TT}+\mathbf{D}_{QS}+\mathbf{D}_{RT}\right)\lambda_y+\mathbf{D}_{SQ}+\mathbf{D}_{TR}, & j=1\\ \mathbf{D}_{RS}\lambda_y^2+\left(\mathbf{D}_{RQ}+\mathbf{D}_{TS}\right)\lambda_y+\mathbf{D}_{TQ}, & j=0\end{cases} \tag{11}$$

The above quadratic eigenproblem can also be converted as shown in [43] into an ordinary linear generalized eigenproblem of twice the size, by defining a new vector $\mathbf{z}=\lambda_y\mathbf{u}_Q$:

$$\begin{bmatrix} -\mathbf{A}_0 & 0 \\ 0 & \mathbf{I} \end{bmatrix} \begin{Bmatrix} \mathbf{u}_Q \\ \mathbf{z} \end{Bmatrix} = \lambda_y \begin{bmatrix} \mathbf{A}_1 & \mathbf{A}_2 \\ \mathbf{I} & 0 \end{bmatrix} \begin{Bmatrix} \mathbf{u}_Q \\ \mathbf{z} \end{Bmatrix} \tag{12}$$

with **I** the identity matrix. The propagating wavenumbers are then calculated as:

$$\kappa_x = \mathrm{i}\frac{\log(\lambda_x)}{d_x} \tag{13a}$$

$$\kappa_y = \mathrm{i}\frac{\log(\lambda_y)}{d_y} \tag{13b}$$

The process of correlating the computed wavenumbers for each frequency and each direction of propagation is straightforward [14]. The corresponding phase and group velocities for each computed wave can be extracted as:

$$y_{\omega_k}^{model}(\boldsymbol{\theta}) = \begin{cases} c_p = \dfrac{\omega_k}{\kappa} \\ c_g = \dfrac{\mathrm{d}\omega_k}{\mathrm{d}\kappa} \end{cases} \tag{14}$$

which form the matrix of angle and frequency dependent modelled data. The Lamb wave types of interest can directly be identified through their corresponding waveforms contained in the eigenvectors $\mathbf{u}_Q$. It should be noted that the above approach can account for calculations with regard to structures having their material principal axes not aligned with the system coordinates. Energy skewing (phase velocities and group velocities having different propagation angles) can also be accounted for as described in [44], but inclusion of these phenomena is out of scope for the current manuscript and will not be investigated in the elaborated case studies.

2.2 Experimental process for extracting wave characteristics

The primary focus of this study is to recover structural parameters of layered composites by experimentally observing local wave data measured on the assembled layered structure. As a result, the measurements serve as the basis of making inference about the parameters of a mathematical model. The required data to be extracted and later fed into the structural identification process of this study are the wave phase or group velocities of specific wave types propagating within the laminate under investigation. A number of methods can be employed for exciting and measuring specific wave propagation modes within a composite structure, such as piezoelectric transducers or non-contact laser actuation in the ultrasound frequency range. A major advantage of employing wave-based identification is that velocities can be measured locally, therefore providing a full description of the structural properties within a specified desired area. This is in contrast to global non-destructive approaches (i.e. modal methods) which struggle to robustly identify local structural properties especially with regard to multilayer structures. The information can be collected either through standard portable ultrasound equipment or through permanently bonded actuators and sensors attached on the structure under investigation.

In this paper, ultrasonic data are obtained from two different sources: (1) numerical simulations using finite element models, and (2) real experiments by making use of standard equipment, e.g. arbitrary waveform generators and oscilloscopes. In (1), sensors can be placed at any arbitrary node of the mesh of the structure. This enables a high number of virtual sensors to be used, which in turn demands an efficient, accurate, and rigorous method to extract the wave dispersion characteristics, e.g. by a two-dimensional Fourier transform (2D-FFT) [45]. Oppositely, in (2), a limited number of sensors can be placed in the structure in practice, and therefore a different approach to obtain group velocities is used by means of a Hilbert transform [46].

2.2.1 Phase velocity extraction for numerical measurements

The 2D-FFT is a technique used to obtain dispersion characteristics of multimode signals [45]. It requires N measurements from sensors evenly spaced along a line, i.e. simulating a B-Scan. Given the flexibility that a finite element model provides, virtual sensors are placed relatively closed to each other so that a high amount of data is collected. The resolution of such 2D-FFT depends, among other factors, on the number of sensors used in the B-Scan. As a result, the dispersion characteristics of the guided waves are obtained by means of wavenumbers κ and frequencies ω_k. Finally, phase velocities are calculated by dividing the angular frequencies by the wavenumbers:

$$y_{\omega_k}^{mea} = \frac{\omega_k}{\kappa} \tag{15}$$

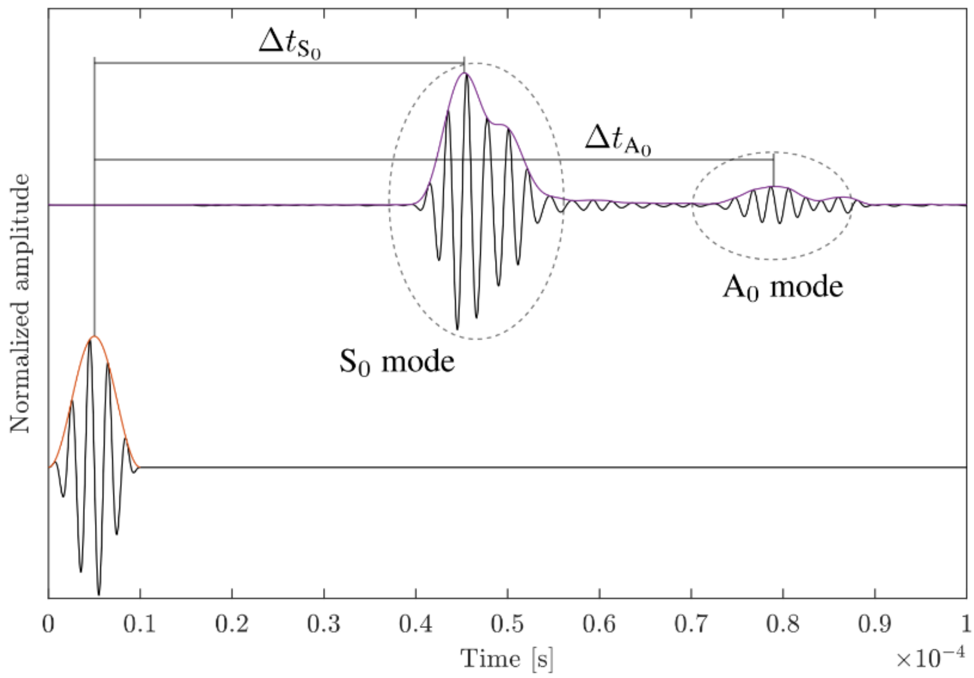

Fig. 2: Excitation signal at $x = x_0$ (below) and the received signal at $x = x_1$ (above) with their corresponding envelopes as computed by the Hilbert transform.

2.2.2 Group velocity extraction for experimental measurements

For extracting the wave propagation velocity of different modes, excited in the experiments, the established Hilbert transform [46] will be employed. Assume that the waveguide is excited at a specific central frequency ω_k at a location $x = x_0$ and the signal is monitored at a location $x = x_1$, after which the signal has travelled over a distance of $L = x_1 \text{-} x_0$. Time histories are initially registered at the excitation and monitoring locations. The signal envelope is determined at emission, $x = x_0$ and reception, $x = x_1$ while the time delay is defined by the time difference between the maximal amplitudes of the envelopes. The local amplitudes of the time history signal $x(t)$ are obtained from the Hilbert Transforms $H\left[x(t)\right]$ of the acquired signals in the time domain:

$$X(t) = \frac{1}{\pi} P \int_{-\infty}^{+\infty} \frac{x(t')}{t-t'} dt' \tag{16}$$

Thus, the wave-packets corresponding to each mode can be identified in the time-domain signal, and by applying the Hilbert transform, the time-of-flight (ToF) can be measured with respect to the maximum amplitude of the wave-packet of interest. As shown in Fig. 2, in order to obtain the real ToF of a wave-packet from the actuator to the sensor, the difference of time of flight $\Delta t|_{\omega_k}$ in both the actuator and the sensor is considered. S0 denotes the first symmetric mode while A0 denotes the first anti-symmetric mode. Note that Fig. 2 depicts two signals, one for the actuation and one for reception of GW, which illustrate the estimation process of the time of flight of both the S0 and A0 wave modes. Therefore, the wave propagation velocity of each mode $y_{\omega_k}^{mea}$ can be obtained from its ToF and its propagation distance L:

$$y_{\omega_k}^{mea} = \frac{L}{\Delta t|_{\omega_k}} \tag{17}$$

This procedure can be repeated for the different signals acquired at different excitation frequencies. In real application, the measurement noise $y_{\omega_k}^{mea}$ is inevitable and it should be modelled as a random variable, to be shown in Eq. (26).

3 Bayesian Inference with a WFE-aided Metamodeling Scheme

Bayesian inference usually requires repeated evaluations of the likelihood function and consequently numerous runs of the forward solver to predict the model responses, i.e., phase and group velocities in this study. An expensive stochastic simulation in Bayesian inference may make the procedure unaffordable. To address this issue, a fast Bayesian inference scheme based on WFE-aided metamodeling is proposed in this section and the main procedures are outlined as follows:

(a) Generation of training inputs $\boldsymbol{\Theta}$

- Generate the sampling points of the parameters $\boldsymbol{\Theta}=\left\{\boldsymbol{\theta}^{(1)},\boldsymbol{\theta}^{(2)},\cdots,\boldsymbol{\theta}^{(n_s)}\right\}^T$ by using proper design of experiments (DoE);

(b) Creation of training outputs database $\mathrm{G}_{\omega_k}(\boldsymbol{\Theta})$

- Compute the wave properties $\mathrm{G}_{\omega_k}(\boldsymbol{\Theta})=\left\{y_{\omega_k}^{model}\left(\boldsymbol{\theta}^{(1)}\right),y_{\omega_k}^{model}\left(\boldsymbol{\theta}^{(2)}\right),\cdots,y_{\omega_k}^{model}\left(\boldsymbol{\theta}^{(n_s)}\right)\right\}^T$ at each frequency point for each sample input $\boldsymbol{\theta}^{(i)}$ using the WFE scheme; It is worth noting that the procedure should be repeated for different modes of wave properties at different frequency points under concern;

(c) Establishment of a metamodel $\eta_{\omega_k}(\boldsymbol{\theta})$

- Construct Kriging predictor $\eta_{\omega_k}(\boldsymbol{\theta})$ to provide a surrogate mapping between the wave properties $\mathrm{G}_{\omega_k}(\boldsymbol{\Theta})$ and the sampling points $\boldsymbol{\Theta}$;

(d) Realization of Bayesian inference formulism

- Formulate the likelihood function by embedding the measured wave characteristics $y_{\omega_k}^{mea}$ and those predicted by the metamodel $\eta_{\omega_k}(\boldsymbol{\theta})$ in a probabilistic model;

(e) Posterior density estimation with TMCMC

- TMCMC adapted to peaked target PDF is used to estimate the posterior probability distribution of the identified parameters.

3.1 Generation of training inputs $\boldsymbol{\Theta}$

To construct a Kriging predictor, it requires initial DoE to generate samples referenced as the training set. Appropriate DoE plays a vital role in constructing a high-fidelity metamodel because DoE influences the creation of the most informative training data. A number of feature values from the experiment ran across the parameter domain are fit with a metamodel. The term "experiment" herein refers to computer experiments. The selection of sample points should trade off the accuracy and cost of a metamodel to be constructed. Less sample points may reduce the accuracy of the metamodel, while more sample points may improve the accuracy of the surrogate model but increase the computational burden. In real application, the sample points mainly depend on the problem to be solved, the response feature values of interest and the selected method of DoE [47].

In this study, the Latin Hypercube Sampling (LHS) which guarantees to spread design points evenly across each input parameter dimension will be used for the training design [48,49]. In the context of statistical sampling, a Latin hypercube is the generalization of this concept to an arbitrary number of dimensions, whereby each sample is the only one in each axis-aligned hyperplane containing it. LHS aims to spread the sample points more evenly across all possible values [48,49]. We assume that vectors of independent input parameters $\boldsymbol{\Theta}=\left\{\boldsymbol{\theta}^{(1)},\boldsymbol{\theta}^{(2)}\cdots\boldsymbol{\theta}^{(n_s)}\right\}^T$ with $\boldsymbol{\theta}^{(i)}\in\mathbb{R}^{n_p\times 1}$ are selected by using the LHS strategy. Here n_s and n_p denote the number of DoE samples and the number of mechanical parameters to be identified. When sampling a function of n_p variables, it partitions each input distribution into n_s equally probable intervals, and selects one sample from each interval. n_s sample points are then placed to satisfy the Latin hypercube requirements. It shuffles the sample for each input so that there is no correlation between the inputs. This independence is one of the main advantages of this sampling scheme. Another advantage is that random samples can be taken one at a time, remembering which samples were taken so far [49].

3.2 Generating training outputs $\mathrm{G}_{\omega_k}\left(\Theta\right)$

With the training set at hand, one can then calculate the predicted values of the metamodel at various sample points in the parameter space by performing an "experiment" at each of those samples based on the WFE scheme introduced in Section 2.1. The WFE is run at each point $\boldsymbol{\theta}^{(i)}$ in the training design, yielding a vector of training data outputs $\mathrm{G}_{\omega_k}\left(\boldsymbol{\Theta}\right)=\left\{y_{\omega_k}^{model}\left(\boldsymbol{\theta}^{(1)}\right),y_{\omega_k}^{model}\left(\boldsymbol{\theta}^{(2)}\right),\cdots,y_{\omega_k}^{model}\left(\boldsymbol{\theta}^{(n_s)}\right)\right\}^T$ with $y_{\omega_k}^{model}\left(\boldsymbol{\theta}^{(i)}\right)\in\mathbb{R}^{n_p\times 1}$ denoting responses of the system at $\boldsymbol{\theta}^{(i)}$, i.e. the wave characteristics in this study. A number of output values obtained from the "experiment" running across the parameter domain are employed to fit a Kriging model using the ooDACE toolbox [50,51].

3.3 Establishment of the metamodel $\eta_{\omega_k}\left(\boldsymbol{\theta}\right)$

Basically, for any input vector $\boldsymbol{\theta}$, the Kriging predictor of the wave characteristics at an arbitrary frequency ω_k is composed of two parts [51]:

$$\eta_{\omega_k}\left(\boldsymbol{\theta}\right)=f_{\omega_k}\left(\boldsymbol{\theta}\right)+\vartheta_{\omega_k}\left(\boldsymbol{\theta}\right) \tag{18}$$

where $f_{\omega_k}\left(\boldsymbol{\theta}\right)$ denotes a regression function constructed based on the data which are usually pre-scribed in real applications, and $\vartheta_{\omega_k}\left(\boldsymbol{\theta}\right)$ denotes a Gaussian process constructed through the residuals. The idea is that the regression function captures the largest variance in the data (the general trend) and that the Gaussian Process interpolates the residuals.

For a set of n_s samples $\boldsymbol{\Theta}=\left\{\boldsymbol{\theta}^{(1)},\boldsymbol{\theta}^{(2)},\cdots,\boldsymbol{\theta}^{(n_s)}\right\}^T$ in n_p dimensions, $\eta_{\omega_k}(\boldsymbol{\theta})=\mathrm{G}_{\omega_k}(\Theta)$, while the Gaussian stationary process $\vartheta_{\omega_k}(\Theta)$ has a zero mean and the covariance matrix modeled as [51]:

$$\mathrm{Cov}\left(\vartheta_{\omega_k}(\Theta)\right)=\sigma_{\omega_k}^2\boldsymbol{Y}_{\omega_k}(\Theta) \tag{19}$$

where $\sigma_{\omega_k}^2$ is the variance and $\boldsymbol{Y}_{\omega_k}$ is a parametric correlation function defined by:

$$\boldsymbol{Y}_{\omega_k}(\Theta)=\begin{bmatrix} \varphi\left(\boldsymbol{\theta}^{(1)},\boldsymbol{\theta}^{(1)}\right) & \cdots & \cdots & \cdots & \varphi\left(\boldsymbol{\theta}^{(1)},\boldsymbol{\theta}^{(n_s)}\right) \\ \vdots & \ddots & \vdots & \iddots & \vdots \\ \vdots & \cdots & \varphi\left(\boldsymbol{\theta}^{(p)},\boldsymbol{\theta}^{(q)}\right) & \cdots & \vdots \\ \vdots & \iddots & \vdots & \ddots & \vdots \\ \varphi\left(\boldsymbol{\theta}^{(n_s)},\boldsymbol{\theta}^{(1)}\right) & \cdots & \cdots & \cdots & \varphi\left(\boldsymbol{\theta}^{(n_s)},\boldsymbol{\theta}^{(n_s)}\right) \end{bmatrix} \tag{20}$$

where $\varphi\left(\boldsymbol{\theta}^{(p)},\boldsymbol{\theta}^{(q)}\right)\left(p,q=1,2,\cdots,n_s\right)$ denotes the correlation function parametrized by a set of hyperparameters, which can be identified by maximum likelihood estimation [50,51]. A classical common choice for this correlation function is the exponential correlation function allowing controlling both the range of influence and the smoothness of the approximation function [51]:

$$\varphi\left(\boldsymbol{\theta}^{(p)},\boldsymbol{\theta}^{(q)}\right)=\prod_{j=1}^{n_p}\exp\left(-\upsilon_j\left|\boldsymbol{\theta}_j^{(p)}-\boldsymbol{\theta}_j^{(q)}\right|^{\delta}\right) \tag{21}$$

while υ_j describes the influence sphere of a point on nearby points for each dimension, i.e., how fast the correlation drops to zero; the parameter δ determines the initial drop in correlation as distance increases. When $\delta=2$, Eq. (21) reduces to the Gaussian correlation function. These correlation functions only depend on the distance between the two points

$\boldsymbol{\theta}^{(p)}$ and $\boldsymbol{\theta}^{(q)}$. The smaller the distance between two points indicates the higher the correlation $\boldsymbol{\theta}^{(p)}$ and $\boldsymbol{\theta}^{(q)}$. Therefore, the more the prediction of one point is influenced by the other, i.e., their function values are closer together. Similarly, if the distance increases the correlation drops to zero [50,51]. The hyperparameters υ_j can be obtained by maximizing a likelihood function.

Subsequently, the Kriging predictor $\eta_{\omega_k}\left(\boldsymbol{\theta}^*\right)$ at a new sample point $\boldsymbol{\theta}^* \notin \Theta$ leads to an estimate that is a Gaussian random variable with mean $\mu_{\omega_k}\left(\boldsymbol{\theta}^*, \Theta\right)$ and standard deviation $\mathrm{S}_{\omega_k}\left(\boldsymbol{\theta}^*, \Theta\right)$, that is:

$$\eta_{\omega_k}\left(\boldsymbol{\theta}^*\right) \sim \mathrm{N}\left(\mu_{\omega_k}\left(\boldsymbol{\theta}^*, \Theta\right), \mathrm{S}_{\omega_k}\left(\boldsymbol{\theta}^*, \Theta\right)\right) \tag{22}$$

with

$$\mu_{\omega_k}\left(\boldsymbol{\theta}^*, \Theta\right) = f\, f_{\omega_k}\left(\boldsymbol{\theta}^*\right) + \mathrm{R}_{\omega_k}\left(\boldsymbol{\theta}^*, \Theta\right)^{\mathrm{T}} \boldsymbol{Y}_{\omega_k}^{-1}\left(\Theta\right)\left(\mathrm{G}_{n_s}\left(\Theta\right) - \mathbf{f}_{n_s}\left(\Theta\right)\right) \tag{23a}$$

$$\mathrm{S}_{\omega_k}^2\left(\boldsymbol{\theta}^*, \boldsymbol{\Theta}\right) = \sigma_{\omega_k}^2\left(1 - \mathrm{R}_{\omega_k}\left(\boldsymbol{\theta}^*, \Theta\right)^{\mathrm{T}} \boldsymbol{Y}_{\omega_k}^{-1}\left(\Theta\right)\mathrm{R}_{\omega_k}\left(\boldsymbol{\theta}^*, \Theta\right)\right) \tag{23b}$$

where

$$\mathrm{R}_{\omega_k}\left(\boldsymbol{\theta}^*\right) = \left[\varphi\left(\boldsymbol{\theta}^*, \boldsymbol{\theta}^{(1)}\right), \quad \cdots \quad, \quad \varphi\left(\boldsymbol{\theta}^*, \boldsymbol{\theta}^{(n_s)}\right)\right]^{\mathrm{T}} \tag{24a}$$

$$\mathrm{G}_{\omega_k}\left(\Theta\right) = \left\{y_{\omega_k}^{model}\left(\boldsymbol{\theta}^{(1)}\right), y_{\omega_k}^{model}\left(\boldsymbol{\theta}^{(i)}\right), \cdots, y_{\omega_k}^{model}\left(\boldsymbol{\theta}^{(n_s)}\right)\right\}^T \tag{24b}$$

$$\mathbf{f}_{n_s}\left(\Theta\right) = \left[f_{\omega_k}\left(\boldsymbol{\theta}^{(1)}\right), \quad \cdots \quad, \quad f_{\omega_k}\left(\boldsymbol{\theta}^{(n_s)}\right)\right] \tag{24c}$$

The details of Kriging surrogate model are omitted and interested readers are referred to [51-55]. It is worth noting that the wave properties are vector-valued functions in terms of frequency ω_k, which inevitably change when frequency varies.

3.4 Realization of Bayesian inference formalism

A Bayesian inference procedure is based on the well-known Bayes' theorem, with its general formulation given as [17]:

$$p\left(\varpi \middle| \mathrm{M}, \mathcal{D}\right) = \frac{p\left(\mathcal{D} \middle| \mathrm{M}, \varpi\right) \cdot p\left(\varpi \middle| \mathrm{M}\right)}{p\left(\mathcal{D} \middle| \mathrm{M}\right)} \tag{25}$$

where $p(\mathcal{D}|\mathrm{M})=\int_{\Theta} p\left(\mathcal{D}\middle|\mathrm{M},\varpi\right)\cdot p\left(\varpi\middle|\mathrm{M}\right)\cdot d\varpi$. In above equation, $p\left(\varpi\middle|\mathrm{M},\mathcal{D}\right)$, $p\left(\varpi\middle|\mathrm{M}\right)$ and $p\left(\mathcal{D}\middle|\mathrm{M},\varpi\right)$ denote the posterior distribution, the prior distribution and the likelihood function; ϖ denote the value of the model parameters including the calibration parameters $\boldsymbol{\theta}$ and prediction-error parameters; $\mathcal{D}$ is the available data (i.e. the wave velocity estimates), and M is the model class.

In the context of Bayesian inference, the statistical inference can be executed by embedding the "deterministic" structural models within a class of probability models so that the structural models give a predictable ("systematic") part and the prediction error is modeled as an uncertain ("random") part [56-58]. As is seen in Eq.(23), the model output at arbitrary $\boldsymbol{\theta}^*$ is replaced by a Kriging surrogate model, whose output should follow Gaussian distribution, i.e., $\eta_{\omega_k}\left(\boldsymbol{\theta}^*\right) \sim \mathrm{N}\left(\mu_{\omega_k}\left(\boldsymbol{\theta}^*, \Theta\right), \mathrm{S}^2_{\omega_k}\left(\boldsymbol{\theta}^*, \Theta\right)\right)$. To include the valuable uncertainty information of the predictor, $\eta_{\omega_k}\left(\boldsymbol{\theta}^*\right)$ can be replaced by a random value $\mu_{\omega_k}\left(\boldsymbol{\theta}^*\right)+\chi_{\omega_k}\left(\boldsymbol{\theta}^*\right)$, where $\mu_{\omega_k}\left(\boldsymbol{\theta}^*\right)$ is the mean of Kriging predictor and $\chi_{\omega_k}\left(\boldsymbol{\theta}^*\right)$ is a random variable with the variance $\mathrm{S}^2_{\omega_k}\left(\boldsymbol{\theta}^*\right)$. It is worth mentioning here that the statistics of $\chi_{\omega_k}\left(\boldsymbol{\theta}^*\right)$ can be directly determined from Kriging predictor without any assumptions here. As a result, the measured wave properties $y_{\omega_k}^{mea}$ can be connected with the model parameters $y_{\omega_k}^{mea}$ to be identified as follows [59]:

$$y_{\omega_k}^{mea} = \mu_{\omega_k}\left(\boldsymbol{\theta}^*\right) + \chi_{\omega_k}\left(\boldsymbol{\theta}^*\right) + \varepsilon_{\omega_k} \tag{26}$$

where ε_{ω_k} is an additive white noise representing the measurement noise and model error, modeled by a Gaussian random variable with variance σ_ε^2.

By embedding Eq. (26) into the probabilistic model of $y_{\omega_k}^{mea}$, one can obtain that:

$$p\left(y_{\omega_k}^{mea}\middle|\boldsymbol{\theta}^*, \sigma_\varepsilon^2\right) = \frac{1}{\sqrt{2\pi}\sqrt{\sigma_\varepsilon^2 + \mathrm{S}_{\omega_k}^2\left(\boldsymbol{\theta}^*, \Theta\right)}} \exp\left\{-\frac{1}{2\left(\sigma_\varepsilon^2 + \mathrm{S}_{\omega_k}^2\left(\boldsymbol{\theta}^*, \Theta\right)\right)}\left(y_{\omega_k}^{mea} - \mu_{\omega_k}\left(\boldsymbol{\theta}^*, \Theta\right)\right)^2\right\} \tag{27}$$

As shown by Eq. (27), the uncertainty of the surrogate model has been readily incorporated in the likelihood function.

Assume that the wave characteristics over the frequency band $\mathcal{D}=\left\{y_{\omega_k}^{mea}, k \in \left[k_1, k_2\right]\right\}$ are used as model inputs, then we can formulate the likelihood function $p\left(\mathcal{D}\middle|\mathsf{M}, \varpi\right)$ as:

$$p\left(\mathcal{D}\middle|\mathsf{M}, \varpi\right) = \prod_{k=k_1}^{k_2} p\left(y_{\omega_k}^{mea}\middle|\boldsymbol{\theta}^*, \sigma_\varepsilon^2\right) \tag{28}$$

Here we assume that the measured data at different frequency points are independent. The Bayesian formalism is kept, which allows for a correct evaluation of the posterior uncertainty on the parameters $\boldsymbol{\theta}^*$.

According to the Bayes' theorem, we can condition the prior on the training data and integrate over the prior distribution of the coefficients to obtain the posterior uncertainties of the parameters to be identified $\varpi=\left\{\boldsymbol{\theta}^*, \sigma_\varepsilon^2\right\}$:

$$p\left(\varpi\middle|\mathsf{M}, \mathcal{D}\right) \propto p\left(\varpi\middle|\mathsf{M}\right)\exp\left(-\mathrm{L}\left(\varpi\right)\right) \tag{29}$$

with $\mathrm{L}\left(\varpi\right)$ denoting the negative-log likelihood function given by

$$\mathrm{L}\left(\varpi\right)=\sum_{k=k_1}^{k_2}\left[\frac{1}{2}\ln\left[\sigma_\varepsilon^2+\mathrm{S}_{\omega_k}^2\left(\boldsymbol{\theta}\right)\right]+\frac{1}{2}\frac{\left(y_{\omega_k}^{mea}-\mu_{\omega_k}\left(\boldsymbol{\theta}\right)\right)^2}{\left(\sigma_\varepsilon^2+\mathrm{S}_{\omega_k}^2\left(\boldsymbol{\theta}\right)\right)}\right] \tag{30}$$

As a result, the posterior distribution $p\left(\varpi|\mathrm{M},\mathcal{D}\right)$ of the identification parameters and prediction-error parameters can be estimated using TMCMC algorithm [42] introduced in Section 3.5.

3.5 Posterior density estimation with TMCMC

The posterior distribution $p\left(\varpi|\mathrm{M},\mathcal{D}\right)$ can be estimated through a Laplace asymptotic approximation, which utilizes a Gaussian approximation as the posterior PDF. However, application of this approximation encounters difficulties when the amount of data is small, or the chosen class of models is unidentifiable. Also, such an approximation requires a non-convex optimization in a high-dimensional parametric space, which is computationally challenging, especially when the model class is not globally identifiable and there may be multiple local maxima [60]. In recent years, focus has shifted from analytical approximations to using stochastic simulation methods in which samples consistent with the posterior PDF $p\left(\varpi|\mathrm{M},\mathcal{D}\right)$ are generated. Stochastic simulation can handle more general cases than the asymptotic approximation approach. In such methods, all probabilistic information encapsulated in $p\left(\varpi|\mathrm{M},\mathcal{D}\right)$ is characterized by posterior samples. MCMC simulation methods were among the most popular methods for solving the Bayesian inverse problem efficiently [61,62].

In this study, the TMCMC algorithm [42] will be employed to sample the posterior PDF given in (29). When the support of the posterior PDF in the parameter space has complex geometry or when the posterior PDF is very peaked and isolated in a small region in the parameter space, proper convergence to the posterior PDF can be a serious problem. To address this critical issue, the TMCMC algorithm has been proposed to choose the proper adaptive proposal PDF in MCMC methods for accelerating convergence to the posterior PDF. Compared with the previous approaches, TMCMC has several advantages: (i) it can handle very peaked or very flat PDFs along certain directions in the parameter space efficiently, rendering it capable of calculating multimodal posterior PDFs; (ii) it can estimate the evidence, which is important for Bayesian model class selection [42]. Algorithmic improvements related to TMCMC can be found in [63,64].

TMCMC adopts the idea of using a sequence of intermediate PDFs such that the last PDF in the sequence is $p\left(\varpi \middle| \mathcal{M}, \mathcal{D}\right)$. Re-weighting and re-sampling techniques are adopted on the samples from a target PDF $\pi_i(\varpi)$ to generate initial samples for the next target PDF $\pi_{i+1}(\varpi)$ in the sequence. As an evolutionary strategy, the TMCMC algorithm starts by constructing a series of intermediate probability distributions iteratively [42,65,66]:

$$p_j\left(\varpi \middle| \mathcal{M}, \mathcal{D}\right) = p\left(\varpi \middle| \mathcal{M}\right) \cdot p\left(\mathcal{D} \middle| \mathcal{M}, \varpi\right)^{q_j}, \quad j = 0, \cdots, n_{stage} \tag{31}$$

where $0 = q_0 < q_1 < \cdots < q_{n_{stage}} = 1$. The process mentioned in the above starts by generating samples from the prior probability distribution $p_0\left(\varpi \middle| \mathcal{M}, \mathcal{D}\right) \propto \pi\left(\varpi \middle| \mathcal{M}\right)$, followed by a series of sampling operations for each intermediate stage $j = 0, \cdots, n_{stage}$. Given the N_j samples $\left\{\varpi_{j,k}, k = 1, \cdots, N_j\right\}$ from the intermediate probability distribution $p_j\left(\varpi \middle| \mathcal{M}, \mathcal{D}\right)$ at stage j, one can generate N_{j+1} samples $\left\{\varpi_{j+1,k}, k = 1, \cdots, N_{j+1}\right\}$ from the next PDF $p_{j+1}\left(\varpi \middle| \mathcal{M}, \mathcal{D}\right)$ at stage $j+1$ based on the plausibility weights of the N_j samples drawn from $p_j\left(\varpi|\mathrm{M},\mathcal{D}\right)$ with respect to the probability distribution $p_{j+1}\left(\varpi|\mathrm{M},\mathcal{D}\right)$ [42,65,66]:

$$w(\varpi_{j,k})=\frac{p_{j+1}\left(\varpi_{j,k}|\mathrm{M},\mathcal{D}\right)}{p_j\left(\varpi_{j,k}|\mathrm{M},\mathcal{D}\right)}=\left(p\left(\mathcal{D}|\varpi_{j+1,k},\mathrm{M}\right)\right)^{q_{j+1}-q_j} \tag{32}$$

In order to avoid the repetition of identical elements in the new sample, MCMC steps are applied to disturb the sample while keeping the same distribution. The Metropolis-Hastings algorithm is used to draw the proposals for the MCMC steps: a Gaussian distribution around the previous point of the Markov Chain. Its covariance is estimated from the samples $\varpi_{j,k}$ at the stage j. A factor β is introduced to control the step size. The choice of q_j in Equation (32) controls the transition between adjacent probability distributions, which in turn controls the convergence rate and effectiveness of TMCMC. The Coefficient of Variation (CoV) of the plausibility weights $\mathrm{COV}\left(w(\varpi_{j,k})\right)$ at stage j is a good indicator of the smoothness of this transition. The choice of the q_{j+1} value is controlled automatically by the TMCMC algorithm so that the $\mathrm{COV}\left(w(\varpi_{j,k})\right)\leq tol$, where tol is a prescribed tolerance. Interested readers can be referred to [42,61,62] for more details of TMCMC.

4 Case Studies

4.1 Numerical validation

The accuracy of the proposed algorithm is firstly demonstrated through a numerical simulation of a non-isotropic composite structure comprising three layers, two isotropic ones and one orthotropic. Identification of mechanical properties is to be sought in both principal directions. The mechanical properties of each layer are shown in Table 1. The structure is assumed to be excited by a broadband chirp signal at a 2 MHz central frequency with a range from 1 Hz to 4 MHz during 4μs. A plane strain Abaqus/Explicit model with free boundary conditions and a mesh size of 25 μm is used to extract the ultrasonic signals at 161 consecutive sensing points, which are spaced 0.25mm, as can be appreciated in Fig. 3. Note that the material properties of layer no. 3 are modified to represent both principal directions of the structure so that two simulations are run representing the X and Y directions. The dispersion curves obtained by applying the 2D-FFT allow us to obtain the phase velocities (see Section 2.2) in the main directions (X and Y) as shown in Fig. 4.

Table 1: Mechanical properties of different layers of the composite structure

Layer No.	Mechanical properties	Values
Layer 1	Young's modulus $E_1\left(\text{GPa}\right)$	200
	Poisson ratio	0.1
	Density $\rho_1\left(\text{kg/m}^3\right)$	500
	Thickness $\tau_1\left(\text{mm}\right)$	0.5
Layer 2	Young's modulus $E_2\left(\text{GPa}\right)$	50
	Poisson ratio	0.1
	Density $\rho_2\left(\text{kg/m}^3\right)$	2000
	Thickness $\tau_2\left(\text{mm}\right)$	0.9
Layer 3	Young's modulus $E_{3x}\left(\text{GPa}\right)$	100
	Young's modulus $E_{3y}\left(\text{GPa}\right)$	150
	Poisson ratio	0.1
	Density $\rho_3\left(\text{kg/m}^3\right)$	1000
	Thickness $\tau_3\left(\text{mm}\right)$	1.3

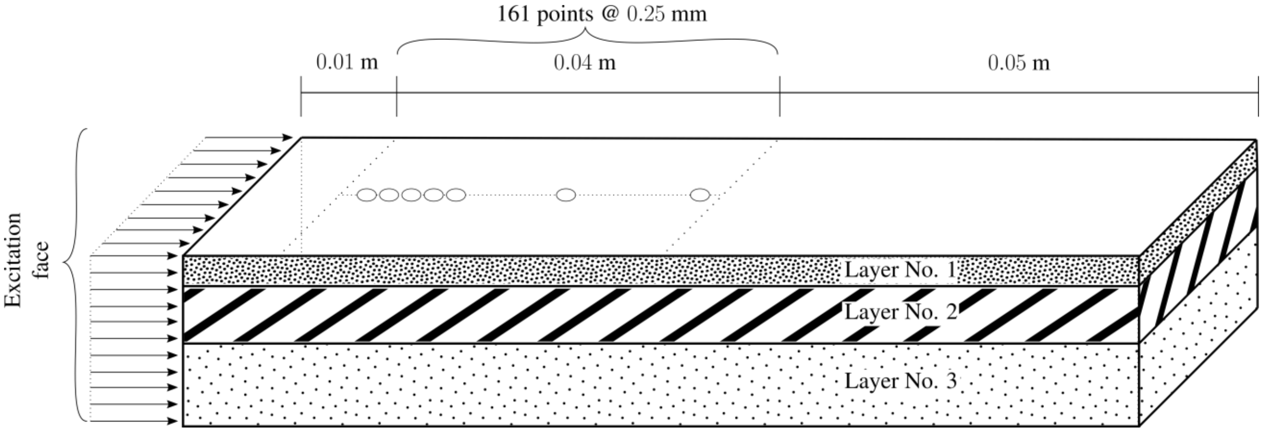

Fig. 3: Schematic of the waveguide of the numerical study.

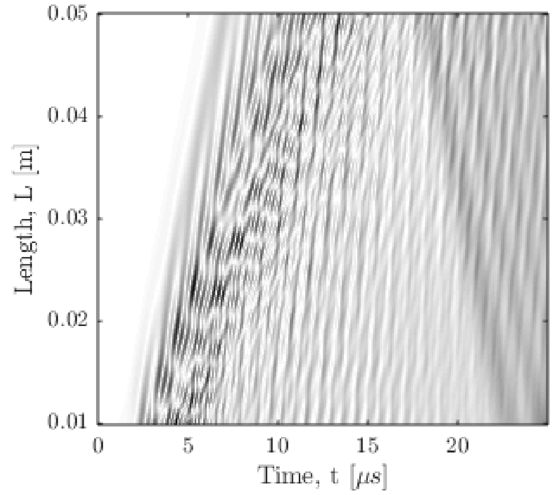

(a) B-Scan in X-direction

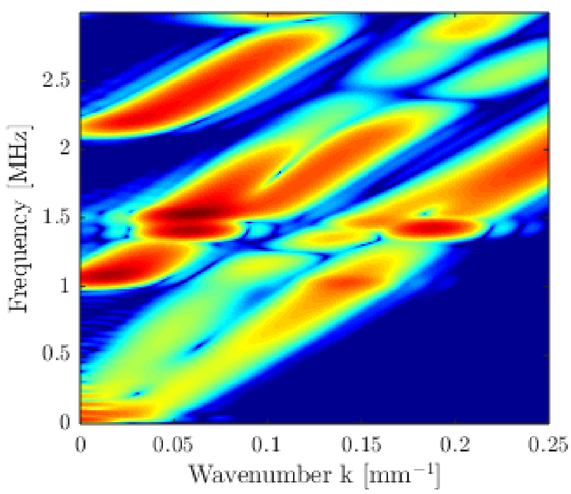

(b) Wavenumbers at X-direction

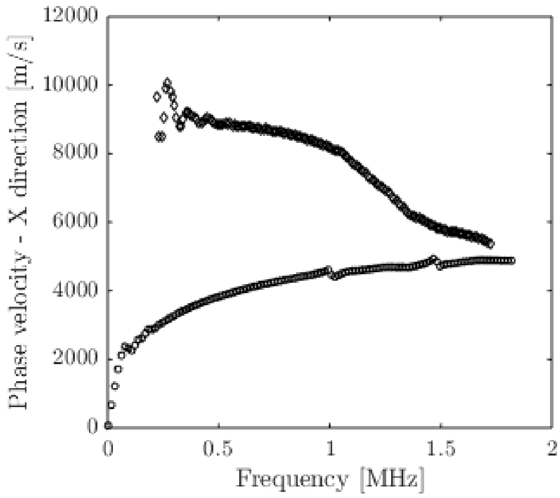

(c) Phase velocities for the symmetric

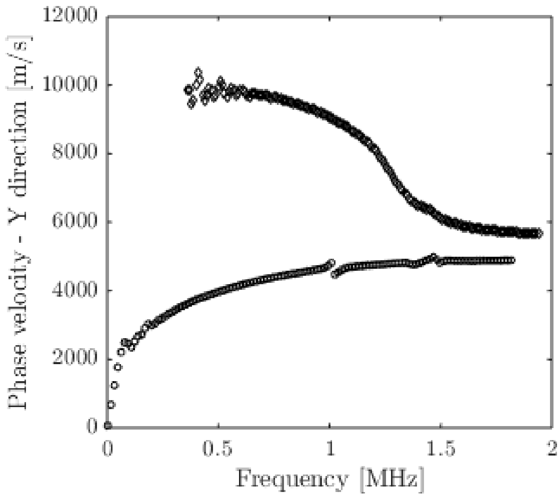

(d) Phase velocities for the symmetric

and antisymmetric Lamb wave modes of the orthotropic layered structures at X direction

and antisymmetric Lamb wave modes of the orthotropic layered structures at Y direction

Fig. 4: Example of a B-Scan acquired at X direction in (a) along with its corresponding 2D-FFT in (b). Besides, wave propagation velocities of the numerical study in X and Y directions are shown in panels (c) and (d), respectively. The diamonds represent the measured velocities of the S0 mode while the circles depict the velocities of the A0 mode.

The parameter vector set to be identified includes $\boldsymbol{\theta}=\left\{E_1, E_2, E_{3x}, E_{3y}, \tau_1, \tau_2, \tau_3\right\}$. Three thousand training points are generated for the parameter $\boldsymbol{\theta}^{(i)}=\left\{E_1^{(i)}, E_2^{(i)}, E_{3x}^{(i)}, E_{3y}^{(i)}, \tau_1^{(i)}, \tau_2^{(i)}, \tau_3^{(i)}\right\}$ $\left(i=1,2,\cdots,3000\right)$ using LHS. For each sampling point, the wave properties corresponding to frequency band shown in Fig. 4 were calculated as training outputs using WFE scheme. The training inputs and outputs are then used for constructing Kriging model between wave properties and the parameters to be identified. The lower and upper bound of the parameters are introduced in Table 2. Then the Bayesian inference is performed by setting the TMCMC parameters as $tol=0.1$, $\beta=0.2$ and $N_j=5000$, resulting in 13 stages in total. The model and the posterior evaluation are entirely written in MATLAB code. We performed the Bayesian inference problem for all scenarios on a multicore server with Intel® Xeon® W-2123 Processor (8.25M Cache, 3.60 GHz) and 32GB of RAM. Based on the WFE-assisted metamodeling scheme, the mechanical properties of the composite structure can be recovered within several minutes. From the analysis, one can draw the following conclusions:

- Fig. 5 presents the convergence diagram of the TMCMC algorithm at different stages, which demonstrates that the proposed algorithm is rather efficient. The histogram of the stochastic samples of the final stage is shown in Fig. 6 accompanied by the kernel density estimation. Results identified using TMCMC including the Most Probable Values (MPV), the mean value and the Coefficient of Variance (COV) are presented in Table 2. As seen in Table 2, the discrepancy between the mean values and the actual values of the mechanical properties of the second and the third layers are less significant. The magnitude of the COV of all identified parameters is around 5-6%. However, a relatively large uncertainty and discrepancy are observed for the mechanical properties of the first layer. Such phenomenon may be attributed to the uncertainty involved in the velocity extracted from the guided wave measurements, approximation using surrogate-kriging modelling, the incompleteness of the information available used for the Bayesian inverse problem, and the complexity nature of the problem. Also, the number of parameters to be identified will also affect the accuracy as it has been well recognized that the performance of MCMC decreases with increasing number of random variables.
- The deterministic method proposed previously [1] is also employed to identify $\boldsymbol{\theta} = \left\{E_1, E_2, E_{3x}, E_{3y}, \tau_1, \tau_2, \tau_3\right\}$. As a deterministic inverse wave and finite element approach, [1] is formulated through a least squares method and solved by using Newton-like iterative scheme. The proposed method in this study significantly outperforms the deterministic approach [1] as the latter fails to get satisfactory results even for the case with less parameters to be identified. The deterministic method can cause divergence

even though the initial guesses are exactly given. As a global optimization approach, the TMCMC algorithm has an important advantage over local optimization as it avoids the need for estimating the initial values of the parameters, which is non-trivial in a number of real engineering problems.

Table 2: Illustration of the identified results using TMCMC

Parameters	Lower bound	Upper bound	Results				
			True	MPV	Mean	Std	COV (%)
E_1 (GPa)	50	400	200	154.301	157.834	10.799	6.842
τ_1 (mm)	0.125	1	0.5	0.665	0.650	0.056	8.552
E_2 (GPa)	12.5	100	50	42.163	42.177	1.982	4.700
τ_2 (mm)	0.225	1.8	0.9	0.751	0.752	0.038	5.118
E_{3x} (GPa)	25	200	100	109.350	106.452	6.022	5.657
E_{3y} (GPa)	25	200	150	147.675	144.036	9.011	6.256
τ_3 (mm)	0.325	2.6	1.3	1.385	1.396	0.092	6.597
σ_ε^2	500	600	-	565.025	561.663	7.062	1.258

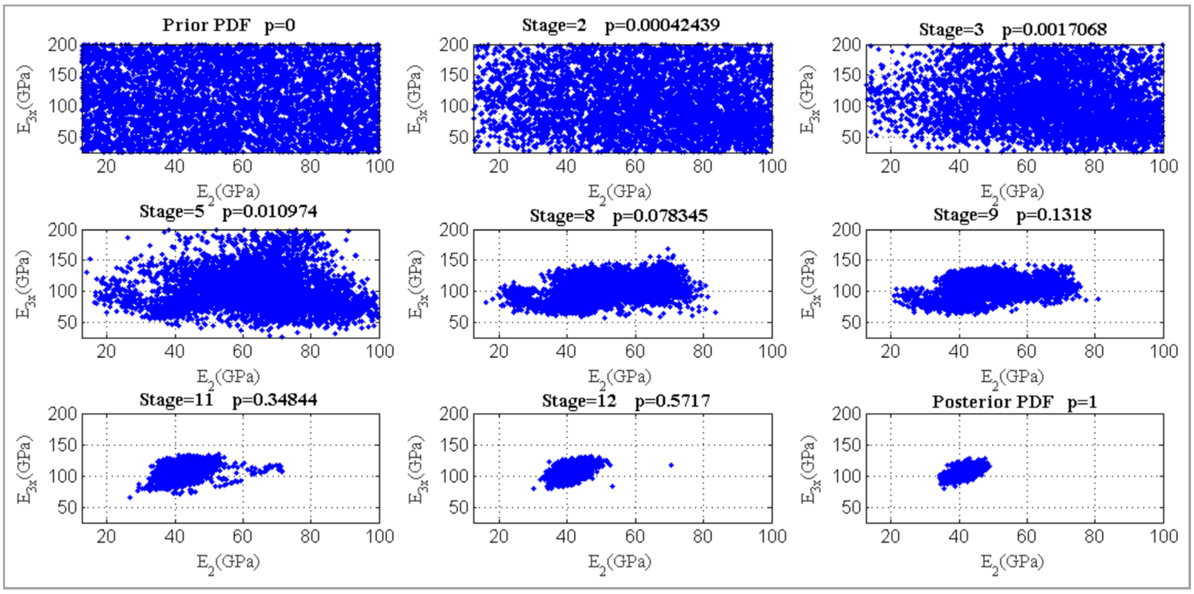

Fig. 5: Convergence diagram of TMCMC at different stages in the plane of E_2 and E_{3x}.

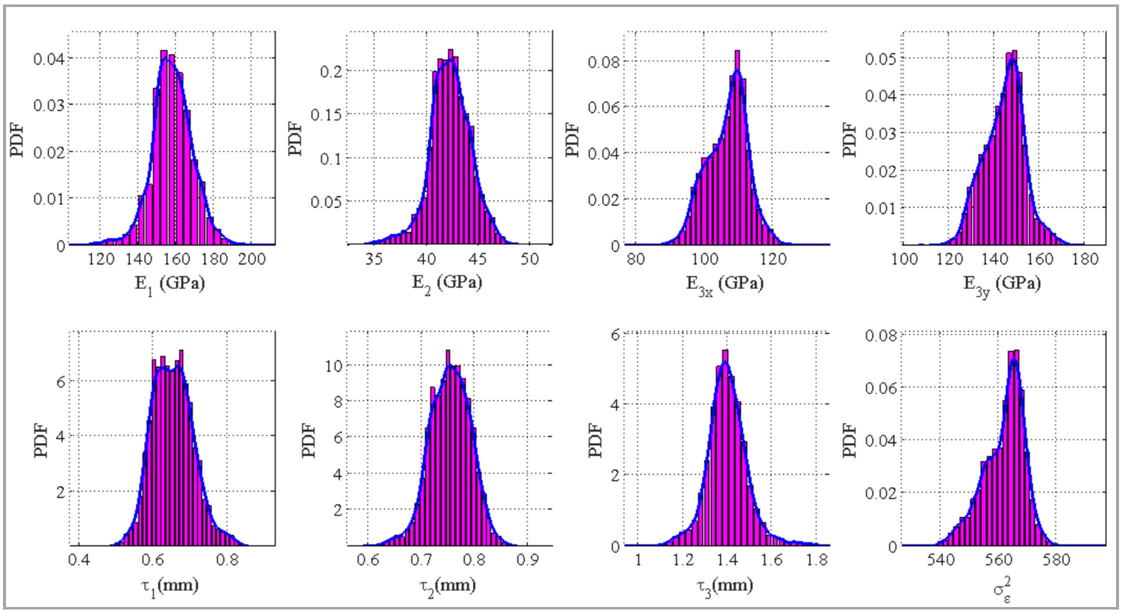

Fig. 6: The histogram of the stochastic samples and its corresponding kernel density estimation for $\varpi = \left\{ E_1, E_2, E_{3x}, E_{3y}, \tau_1, \tau_2, \tau_3, \sigma_\varepsilon^2 \right\}$.

- The variation of posterior uncertainty with the increase of the wave modes and the frequency band of the phase velocity are also investigated in detail. Fig. 7 shows the variation of the posterior COV values with different wave modes involved in the Bayesian inference: (a) S0 mode in the X direction; (b) S0 and A0 modes in the X direction; (c) S0 and A0 mode in the X direction, plus A0 mode in the Y direction; (d) S0 and A0 modes in both X and Y directions. To investigate the effects of frequency bands, part of the frequency band shown in Fig. 2 are considered: (a) first 1/8 frequency band; (b) first 1/4 frequency band; (c) first 1/2 frequency band; (d) 3/4 frequency band; (e) the whole frequency band. Both S0 and A0 modes in two directions are used for identification. Fig. 8 shows the variation of the posterior COV values with the increase of frequency band. Results show that the performance is not satisfactory when only one mode in one direction is available or when the frequency band under concern is too narrow. The COV values of the extracted mechanical properties display a significant decreasing trend with the increase of the number of modes and the frequency band involved for identification. The observations are reasonable and agree well with the intuition as more modes and wider frequency band of wave characteristics indicate more information, less uncertainty and higher identification accuracy.

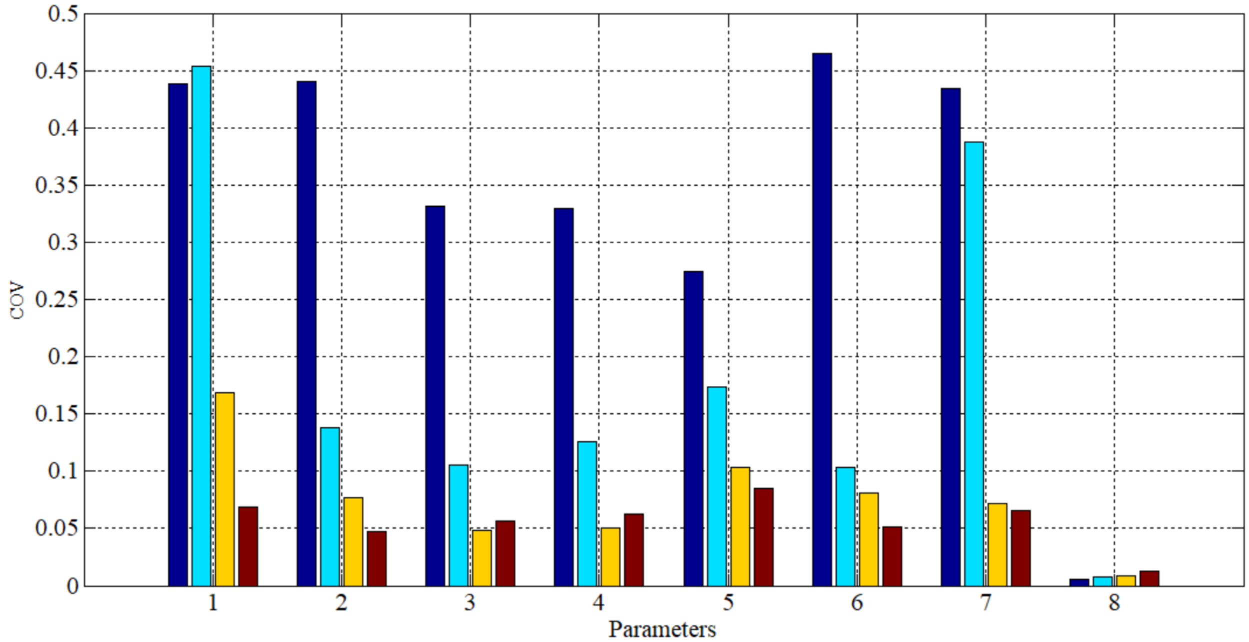

Fig. 7 Variation of posterior COV of mechanical properties with different modes involved in Bayesian inference by considering the following four scenarios: (i) S0 mode in the X direction; (ii) S0 and A0 modes in the X direction; (iii) S0 and A0 mode in the X direction, plus A0 mode in the Y direction; (iv) S0 and A0 modes in both X and Y directions. The number 1-8 along the x axle denotes the parameters $\varpi = \{E_1, E_2, E_{3x}, E_{3y}, \tau_1, \tau_2, \tau_3, \sigma_\varepsilon^2\}$ in order.

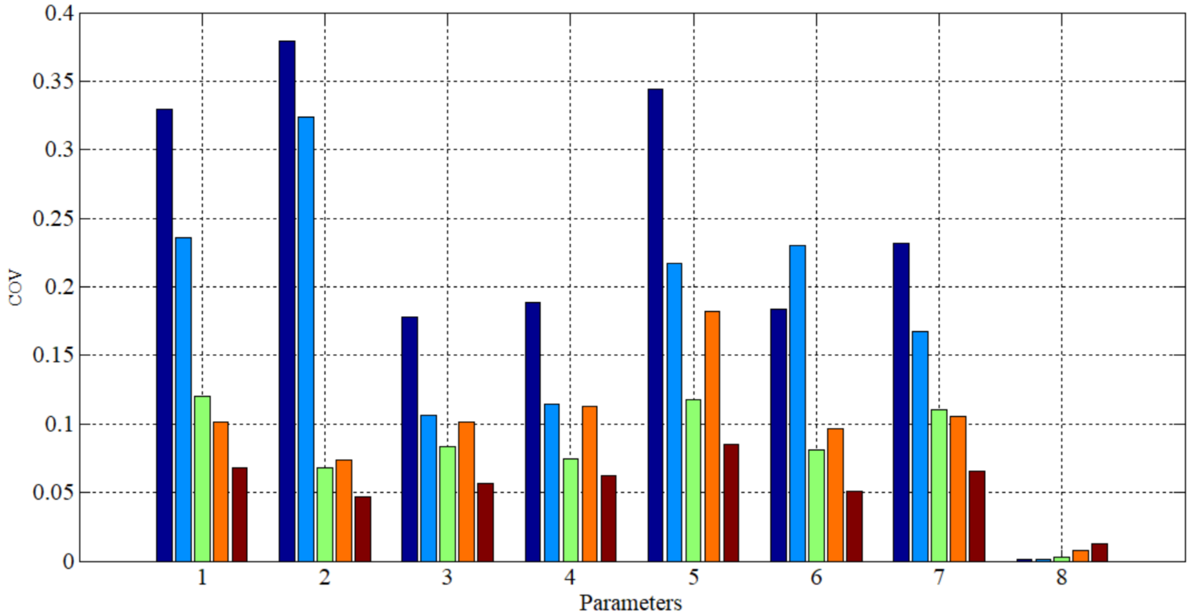

Fig. 8: Variation of posterior COV of mechanical properties with different frequency band of wave characteristics involved in Bayesian inference by considering the following five scenarios: (i) first 1/8 frequency band; (ii) first 1/4 frequency band; (iii) first 1/2 frequency band; (iv) 3/4 frequency band; (v) the whole frequency band. The number 1-8 along the x axle denotes the parameters $\varpi = \{E_1, E_2, E_{3x}, E_{3y}, \tau_1, \tau_2, \tau_3, \sigma_\varepsilon^2\}$ in order.

- If explicit FE simulations without using WFE are employed for Bayesian inference, it is highly non-trivial to achieve the results. For this wave propagation case, the time consumed by the explicit FE method is approximately 1000 times greater than that of the WFE scheme in each run. As a result, the computational effort and the required memory space will increase in an explosive manner compared with the WFE scheme as one has to carry out a large number of runs of full FE scheme within the stochastic simulation, with each run involving the calculation of the wave properties at different frequencies. For more complicated structures, the curse of computational burden will be even worse. Thus, compared with an explicit FE solution, using surrogate approximation in tandem with a WFE scheme can also lead to a drastic reduction in the computational effort.

4.2 Experimental verification

To investigate the feasibility of the proposed method in real applications, two metallic specimens, a 1m×1m aluminum sheet of 1.2mm thickness and a composite structure comprised of a 1m×1m×0.7mm aluminum sheet glued to a 1m×1m×0.8mm steel sheet, were tested to obtain their wave propagation characteristics. To this end, the first symmetric (S0) and anti-symmetric (A0) modes were excited at a range of frequencies from 30 kHz to 1MHz with a step frequency of 10 kHz.

The ultrasonic guided-waves were transmitted using a PZT transducer attached at the center of the specimens using a 5-cycle sine tone burst centered at each frequency, with an amplitude of 8 Vpp. The signals were generated at a Keysight 33512B arbitrary waveform generator, which can be observed in Fig. 9 along with the rest of the experimental setup. The sensor, placed at 200mm from the excitation point, acquired the GWs that were then digitized using a DSOX2014A oscilloscope applying a sampling frequency of 9.6 MHz and an averaging of 32 experiments in order to reduce the system noise. The PZT transducers used in these experiments consisted of circular discs with radial mode vibration (Steminc part number: SMPL7W8T02412WL), which produced a circumferentially even excitation along the surface of the metallic sheets. The velocity results extracted from the experimental measurements and the procedure described in Section 2.2 are depicted in Fig. 10. It can be observed in both the aluminum and composite specimens (Fig. 10a and 10b) that some values of the velocities of the S0 mode are missing due to the low amplitude of that mode in the acquired signals at relatively low frequencies.

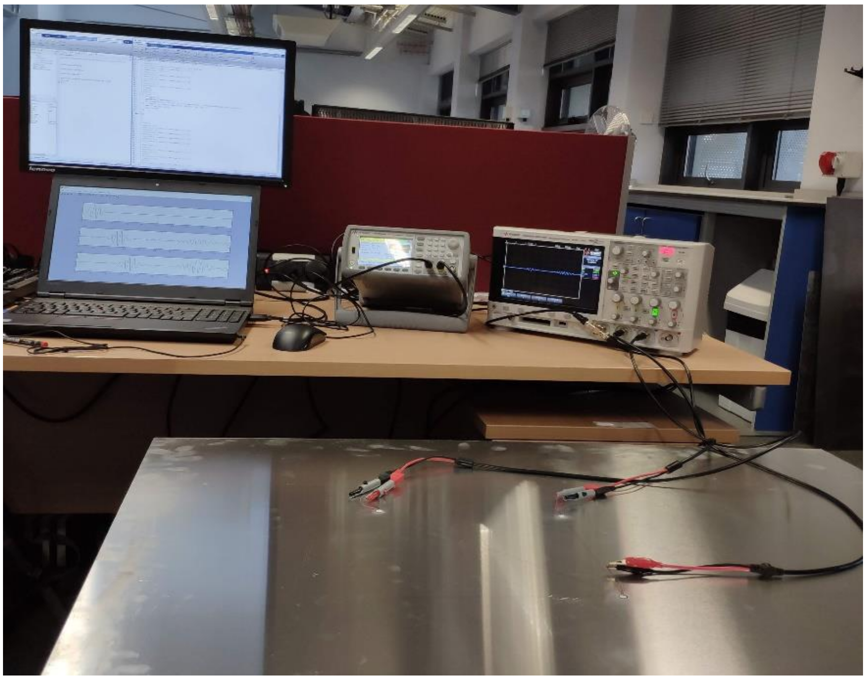

Fig. 9: Experimental suite used comprising a laptop, an arbitrary waveform generator, and an oscilloscope connected to the PZT transducers attached to the metallic specimen.

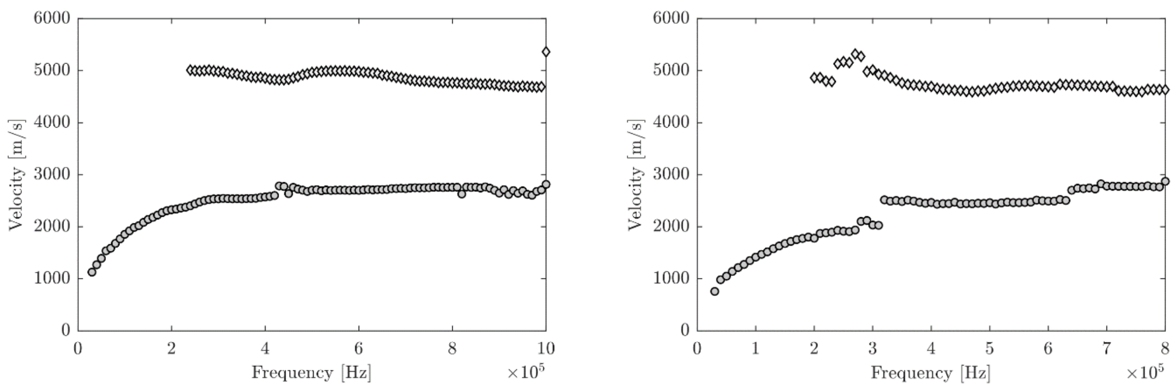

(a) (b)

Fig. 10: Wave propagation velocities of both specimens (a) aluminum and (b) composite. The diamonds represent the measured velocities of the S0 mode while the circles depict the velocities of the A0 mode.

The mechanical properties of the aluminum sheet and the composite structure include $\boldsymbol{\theta}_{alum}=\{E_1,\ \tau_1\}$ and $\boldsymbol{\theta}_{comp}=\{E_1,\ \tau_1, E_2,\ \tau_2\}$. For each specimen, 1500 DoE training points $\boldsymbol{\Theta}=\left\{\boldsymbol{\theta}^{(1)},\boldsymbol{\theta}^{(2)}\cdots\boldsymbol{\theta}^{(1500)}\right\}^T$ are generated as training samples using LHS, the numerical predictions of the velocities of the S0 mode and A0 mode are calculated using the WFE scheme in each computer experiment to formulate the training output data set $\mathrm{G}_{\omega_k}(\Theta)=\left\{y^{model}_{\omega_k}\left(\boldsymbol{\theta}^{(1)}\right), y^{model}_{\omega_k}\left(\boldsymbol{\theta}^{(i)}\right),\cdots, y^{model}_{\omega_k}\left(\boldsymbol{\theta}^{(1500)}\right)\right\}^T$. Here the frequency ω_k should coincide with those of the experimentally measured velocities. The training data $\mathrm{G}_{\omega_k}(\Theta)$ is then used for constructing the Kriging model reflecting the mathematical relationship between the wave properties of the S0 and A0 modes and the structural parameters $\boldsymbol{\theta}$, which will be embedded in the likelihood function for Bayesian inference.

The parameters to be identified include $\varpi_{alum}=\{E_1,\ \tau_1,\sigma_\varepsilon^2\}$ and $\varpi_{comp}=\{E_1,\ \tau_1,E_2,\ \tau_2,\sigma_\varepsilon^2\}$ where σ_ε^2 denotes the prediction-error. A uniform prior distribution was used, and the interval of these parameters are shown in Table 3. $\varpi_{alum} = \{E_1, \tau_1, \sigma_\varepsilon^2\}$ and $\varpi_{comp} = \{E_1, \tau_1, E_2, \tau_2, \sigma_\varepsilon^2\}$ can be obtained by using TMCMC. By setting the TMCMC parameters to be $tolCov = 0.1$ and $N_j = 1000$, the Bayesian inference takes 9 and 12 stages to achieve the posterior uncertainties for two different testing specimen. The evolution of the TMCMC samples through stages in the plane of (E_1, τ_1) for the aluminum sheet and (E_1, E_2) for the composite are shown in Fig. 11(a) and 11(b). It is interesting to see that the samples gradually find the high probability region with increasing stages. The samples converge to the targeted PDF rapidly. The identifiability is clear for the TMCMC samples. Furthermore, it agrees well with the intuition that less stages are required for the first specimen with a smaller number of parameters to be identified.

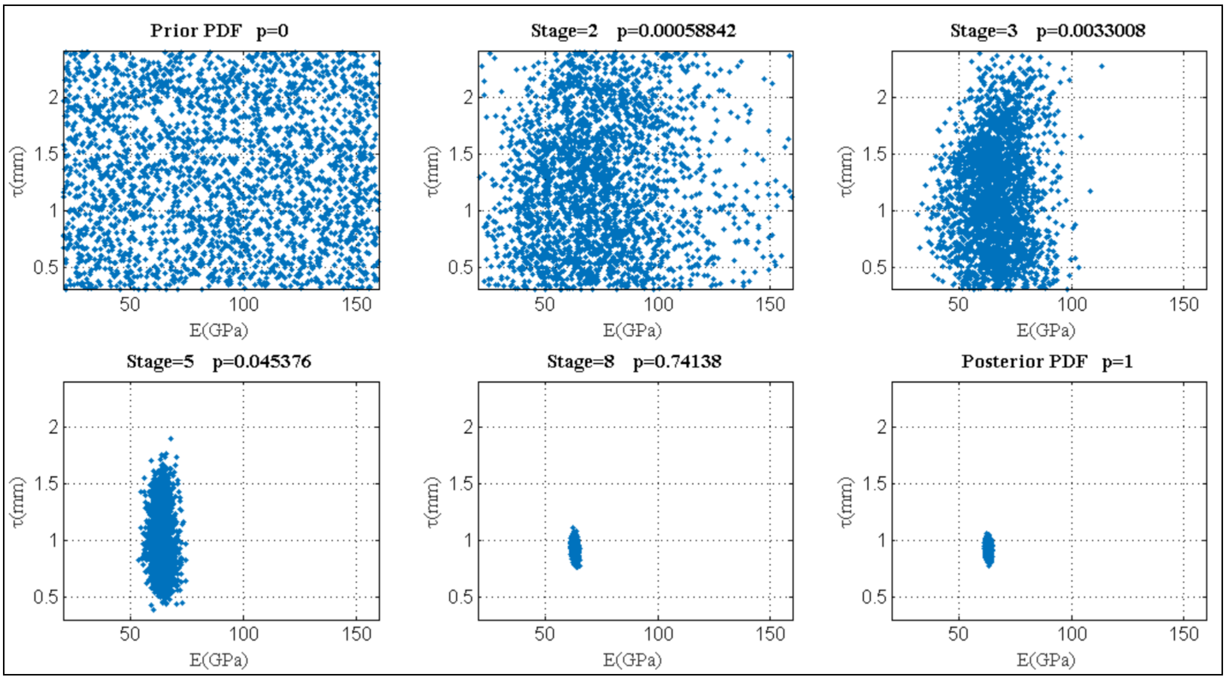

(a) Aluminum specimen

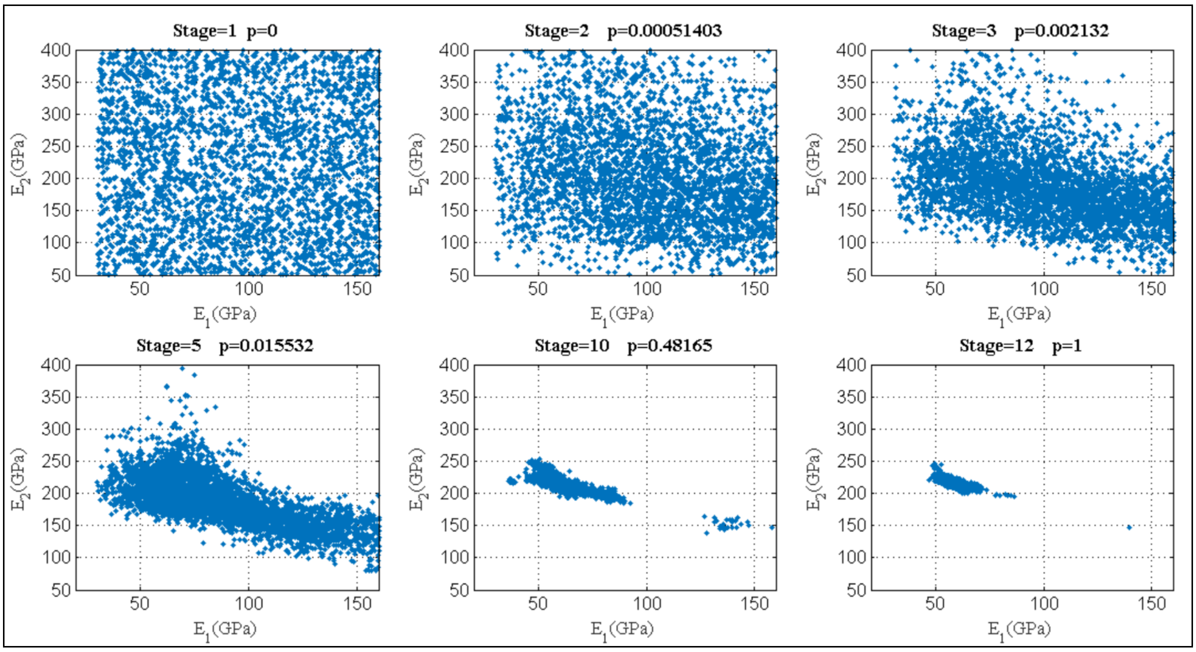

(b) Composite specimen

Fig. 11: Convergence diagram of stochastic samples at different stages in Bayesian inference using TMCMC: (a) (E_1, τ_1) for the aluminum sheet; (b) (E_1, E_2) for the composite.

The mean values and the COV for the aluminum sheet and the composite structure are presented in Table 3. Fig. 12 presents the scatterplot matrices of $\{E_{x1}, \tau_1, \sigma_\varepsilon^2\}$ and $\{E_{x1}, \tau_1, E_{x2}, \tau_2\}$, respectively. Diagonal entries of Fig. 12 denote the marginal distributions of the model parameters estimated using kernel histograms. As observed from Fig. 12, the procedure yields a reasonable capture of the distribution function and all parameters follow uni-modal posterior PDF. The proposed Bayesian approach is able to provide satisfactory results, with median values quite close to those provided by the processing factory as well as identified confidence intervals representing the uncertainties. It is worth mentioning here that the Bayesian inference problem without activating metamodeling strategy produced no results after more than three days’ running of the code. It can be concluded that the WFE-assisted surrogate estimates provide a very fast estimate, making them suitable for using with the TMCMC algorithm. Significant gains in computational effort are achieved without sacrificing the accuracy in the model parameter estimates. However, it is inevitable to discover discrepancy between the identified mechanical properties and the measured mechanical properties, especially for the thickness of the plates. The differences can be attributed to physical uncertainty associated with the manufactured composite structure (e.g. imperfect gluing of the different layers together) as well as the deviation of the velocity extracted from noise-contaminated guided wave measurements.

Table 3: Identified results for the aluminum specimen and the composite specimen

Structural type	Parameters	Interval		Identified values		
		Lower	Upper	Mean	Std	COV (%)
Aluminum specimen	$E\left(\text{Gpa}\right)$	20	160	63.122	0.552	0.88
	$\tau\left(\text{mm}\right)$	0.3	2.4	0.923	0.038	4.2
	σ_{ε}^{2}	100	300	193.441	10.410	5.38
Composite specimen	$E_1\left(\text{Gpa}\right)$	20	160	58.009	3.611	6.225
	$E_2\left(\text{Gpa}\right)$	50	400	216.765	4.904	2.262
	$\tau_1\left(\text{mm}\right)$	0.25	2	0.524	0.020	3.838
	$\tau_2\left(\text{mm}\right)$	0.25	2	0.613	0.016	2.639
	σ_{ε}^{2}	100	200	119.066	7.033	5.907

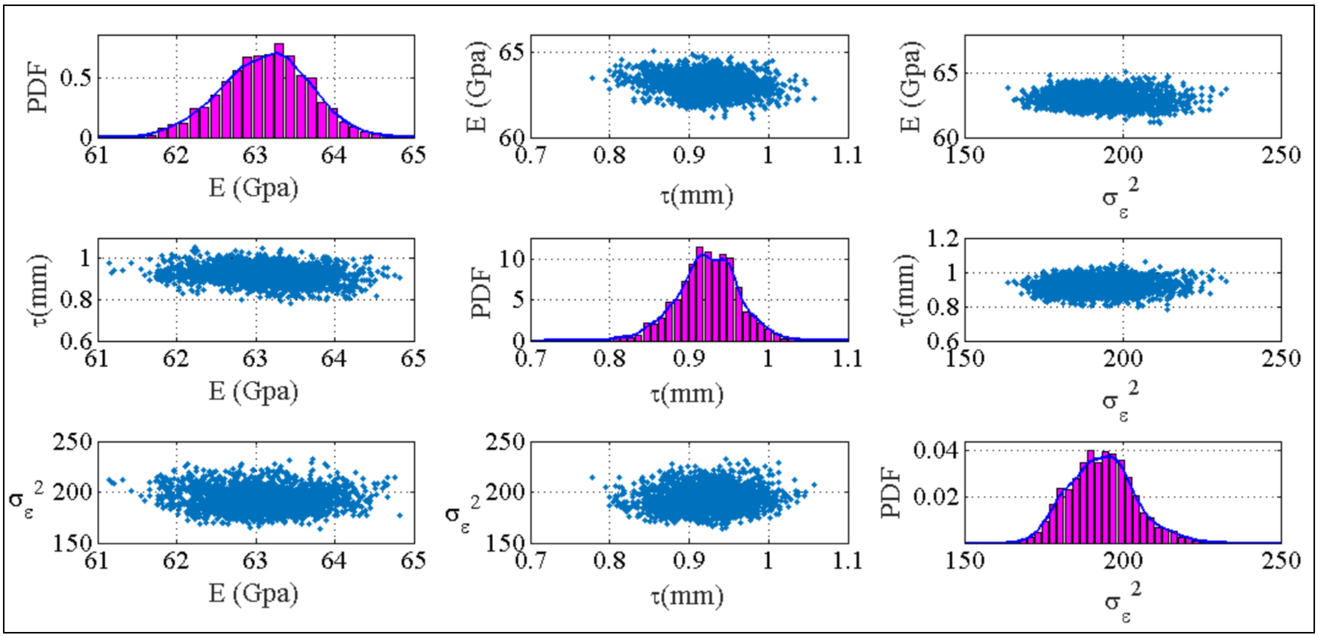

(a)

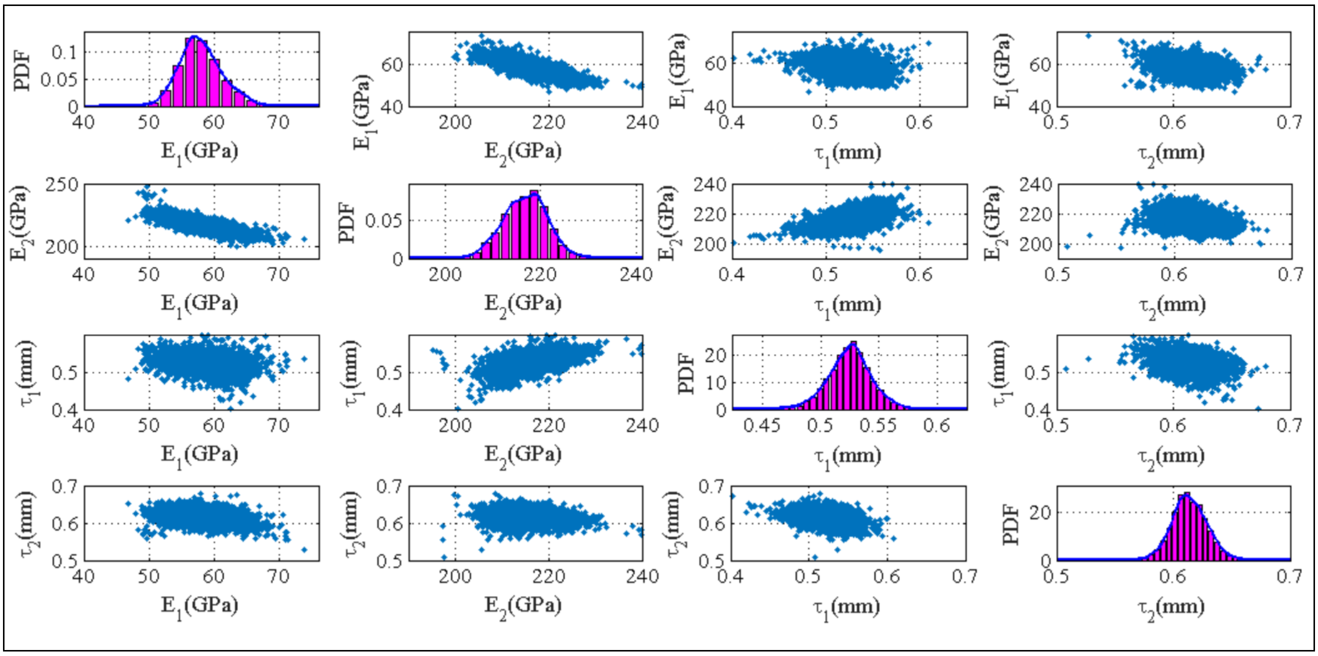

(b)

Fig. 12: Scatterplot matrices of different parameters of the tested specimens: (a) the aluminum sheet; (b) the composite specimen.

5 Conclusions

In this work we have developed and applied a Bayesian identification technique based on FE modelling and the properties of propagating waves in multilayered structures. The principal contribution resulting from this work is a robust numerical nondestructive testing (NDT) procedure for recovering effective structural parameters of layered composites by WFE-aided metamodeling. The propagation constants for the elastic waves travelling are realized through the forward WFE scheme in this study which is preferred to predict the broadband wave properties for layered structures due to its versatility in considering different numbers of layers and complex material properties in a straightforward manner, without the need of altering the forward modelling approach. The computational burden of conventional full FEM analysis scheme is therefore reduced by several orders of magnitude thanks to adoption of the WFE scheme.

In addition, a cheap and fast Kriging surrogate model built using an experiment design strategy in tandem with the WFE scheme is used to avoid a taxiing number of simulations for predicting wave properties and to reduce the computational cost of the repeated likelihood evaluations, as well as the difficulty of interfacing different software environments in stochastic simulation. By establishing the relationship between the training outputs and identification parameters with a statistical method, the Kriging surrogate model removes the need for a large number of repeated FE runs over the procedure of sampling the posterior PDF. As a result, the WFE scheme is only required for training the outputs in the construction of the Kriging model, and is no longer involved in TMCMC, thus significantly enhancing the efficiency and applicability of the presented methodology. The valuable uncertainty information introduced by the use of a surrogate model are also properly taken into account when estimating the parameters' posterior probability distribution.

Case studies were presented to verify the efficiency of the proposed practice. The method is able to extract layer characteristics such as thicknesses and Young's moduli for each individual layer and is robust enough to be applied in a broadband frequency range. In the ultrasound range the wave characteristics are straightforward to extract through the measured wave envelope. The exhibited scheme was validated through comparison with experimental results. Satisfactory agreement is observed for the identified structural parameters. It is emphasized that the proposed wave-based method has significant advantages compared to modal identification approaches. More precisely the accuracy of the structural parameters is not altered by the presence of uncertain boundaries since the data is obtained locally, through single-shot measurements. This is a considerable advantage compared to a number of stationary and other existing methods, since it can then be applied in situ and without requiring additional sampling on structural properties. The use of practically unlimited and user-selected excitation frequencies can effectively increase the number of identifiable parameters through inverse wave modelling, resulting in a significant increase of the method's robustness and applicability in a broadband frequency sense.

Acknowledgments

This research has been supported by the European Union's Horizon 2020 research and innovation Programme under the Marie Skłodowska-Curie Grant Agreement UltraSafe - No. 741284 and the SAFE-FLY project under the Grant Agreement No. 721455, the Natural Science Foundation of China under Award No. 51778203 and the Macau FDCT (File No. SKL-IOTSC-2018-2020 and 019/2016/A1). Also, we are grateful for Prof. Ching for releasing the MATLAB code of TMCMC to the public. The first author would like to express his gratitude to Mr. Shi-Ze Cao for the valuable discussions and kind helps on realizing the TMCMC algorithm.

References

[1] D. Chronopoulos, C. Droz, R. Apalowo, M. Ichchou, W.J. Yan, Accurate structural identification for layered composite structures, through a wave and finite element scheme, Composite Structures 182 (2017) 566-578.

[2] Y. Yang, C.T. Ng, A. Kotousov, H. Sohn, H.J. Lim, Second harmonic generation at fatigue cracks by low-frequency Lamb waves: experimental and numerical studies, Mechanical Systems and Signal Processing 99 (2018)760-773.

[3] C.T. Ng, M. Veidt, A Lamb-wave-based technique for damage detection in composite laminates, Smart materials and structures 18(7) (2009) 074006.

[4] N. Bochud, J. Laurent, F. Bruno, D. Royer, C. Prada, Towards real-time assessment of anisotropic plate properties using elastic guided waves, The Journal of the Acoustical Society of America, 143(2) (2018) 1138-1147.

[5] C. Wang, O. Balogun, J.D. Achenbach, Scattering of a Rayleigh wave by a near surface crack which is normal to the free surface, International Journal of Engineering Science, 145 (2019) 103162.

[6] C. Willberg, S. Duczek, J. Vivar-Perez, Z. Ahmad, Simulation methods for guided wave-based structural health monitoring: A review, Applied Mechanics Reviews 67 (1) (2015) 010803.

[7] J.M. Renno, B.R. Mace, Calculation of reflection and transmission coefficients of joints using a hybrid finite element/wave and finite element approach, Journal of Sound and Vibration 332 (9) (2013) 2149-2164.

[8] R.K. Apalowo, D. Chronopoulos, A wave-based numerical scheme for damage detection and identification in two-dimensional composite structures, Composite Structures 214 (2019) 164-182.

[9] D.J. Mead, A general theory of harmonic wave propagation in linear periodic systems with multiple coupling, Journal of Sound and Vibration 27 (2) (1973) 235-260.

[10] R. Langley, A note on the force boundary conditions for two-dimensional periodic structures with corner freedoms, Journal of Sound and Vibration 167 (1993) 377-381.

[11] B.R. Mace, D. Duhamel, M.J. Brennan, L. Hinke, Finite element prediction of wave motion in structural waveguides, The Journal of the Acoustical Society of America 117 (5) (2005) 2835-2843.

[12] J.M. Mencik, M. Ichchou, Multi-mode propagation and diffusion in structures through finite elements, European Journal of Mechanics-A/Solids 24 (5) (2005) 877–898.

[13] D. Duhamel, B.R. Mace, M.J. Brennan, Finite element analysis of the vibrations of waveguides and periodic structures, Journal of Sound and Vibration 294 (2006) 205–220.

[14] B. Mace, E. Manconi, Modelling wave propagation in two-dimensional structures using finite element analysis, Journal of Sound and Vibration 318 (4-5) (2008) 884–902.

[15] V. Thierry, L. Brown, D. Chronopoulos, Multi-scale wave propagation modelling for two-dimensional periodic textile composites, Composites Part B: Engineering 150 (2018) 144-156.

[16] O.A. Vanli, S. Jung, Statistical updating of finite element model with Lamb wave sensing data for damage detection problems, Mechanical Systems and Signal Processing 42(1-2) (2014)137-151.

[17] J.L. Beck, L.S. Katafygiotis, Updating models and their uncertainties. I: Bayesian statistical framework, Journal of Engineering Mechanics, ASCE 124 (4) (1998) 455-461.

[18] K.V. Yuen, Bayesian Methods for Structural Dynamics and Civil Engineering. John Wiley & Sons, 2010.

[19] K.V. Yuen, S.C. Kuok, Bayesian methods for updating dynamic models, Applied Mechanics Reviews 64 (1) (2011) 010802.

[20] S.K. Au, Operational Modal Analysis: Modeling, Bayesian Inference, Uncertainty Laws, Springer (2017).

[21] W.J. Yan, L.S. Katafygiotis, A novel Bayesian approach for structural model updating utilizing statistical modal information from multiple setups, Structural Safety 52 (2015) 260-271.

[22] W.J. Yan, L.S Katafygiotis, A two-stage fast Bayesian spectral density approach for ambient modal analysis. Part I: posterior most probable value and uncertainty, Mechanical Systems and Signal Processing 54 (2015) 139-155.

[23] W.J. Yan, L.S. Katafygiotis, A two-stage fast Bayesian spectral density approach for ambient modal analysis. Part II: Mode shape assembly and case studies, Mechanical Systems and Signal Processing 54 (2015) 156-171.

[24] H.F. Lam, H.Y. Peng, S.K. Au, Development of a practical algorithm for Bayesian model updating of a coupled slab system utilizing field test data, Engineering Structures 79 (2014) 182-194.

[25] N.H. Paulson, E. Jennings, M. Stan, Bayesian strategies for uncertainty quantification of the thermodynamic properties of materials, International Journal of Engineering Science 142 (2019) 74-93.

[26] S. Doraiswamy, J.C. Criscione, A.R. Srinivasa, A technique for the classification of tissues by combining mechanics based models with Bayesian inference, International Journal of Engineering Science 106 (2016) 95-109.

[27] J.L. Beck, Bayesian system identification based on probability logic, Structural Control and Health Monitoring, 17 (7) (2010) 825-847.

[28] C.T. Ng, Bayesian model updating approach for experimental identification of damage in beams using guided waves, Structural Health Monitoring 13 (4) (2014) 359-373.

[29] C.T. Ng, On the selection of advanced signal processing techniques for guided wave damage identification using a statistical approach, Engineering Structures 67 (2014) 50-60.

[30] S. He, C.T. Ng, A probabilistic approach for quantitative identification of multiple delaminations in laminated composite beams using guided waves, Engineering Structures 127 (2016) 602-614.

[31] S. He, C.T. Ng, Guided wave-based identification of multiple cracks in beams using a Bayesian approach, Mechanical Systems and Signal Processing 84 (2017) 324-345.

[32] G. Yan, A Bayesian approach for damage localization in plate-like structures using Lamb waves, Smart Materials and Structures 22 (3) (2013) 035012.

[33] S. Cantero-Chinchilla, J. Chiachío, M. Chiachío, D. Chronopoulos, A. Jones, A robust Bayesian methodology for damage localization in plate-like structures using ultrasonic guided-waves, Mechanical Systems and Signal Processing 122 (2019) 192-205.

[34] G. Yan, H. Sun, H. Waisman, A guided Bayesian inference approach for detection of multiple flaws in structures using the extended finite element method, Computers & Structures 152 (2015) 27-44.

[35] A.B. Abdessalem, F. Jenson, P. Calmon, Quantifying uncertainty in parameter estimates of ultrasonic inspection system using Bayesian computational framework, Mechanical Systems and Signal Processing 109 (2018) 89-110.

[36] B. Wu, Y. Huang, X. Chen, S. Krishnaswamy, H. Li, Guided-wave signal processing by the sparse Bayesian learning approach employing Gabor pulse model, Structural Health Monitoring 16 (3) (2017) 347-362.

[37] B. Wu, H. Li, Y. Huang, Sparse recovery of multiple dispersive guided-wave modes for defect localization using a Bayesian approach, Structural Health Monitoring 18(4) (2019) 1235-1252.

[38] J. Chiachío, N. Bochud, M. Chiachío, S. Cantero, G. Rus, A multilevel Bayesian method for ultrasound-based damage identification in composite laminates, Mechanical Systems and Signal Processing 88 (2017) 462-477.

[39] J. Yang, J. He, X. Guan, D. Wang, H. Chen, W. Zhang, Y. Liu, A probabilistic crack size quantification method using in-situ Lamb wave test and Bayesian updating, Mechanical Systems and Signal Processing 78 (2016) 118-133.

[40] M.R. Souza, D. Beli, N.S. Ferguson, J.R.D.F. Arruda, A.T. Fabro, A Bayesian approach for wavenumber identification of metamaterial beams possessing variability. Mechanical Systems and Signal Processing, 135 (2020)106437.

[41] W.J. Yan, D. Chronopoulos, C. Papadimitriou, S. Cantero-Chinchilla, G.S. Zhu, Bayesian inference for damage identification based on analytical probabilistic model of scattering coefficient estimators and ultrafast wave scattering simulation scheme. Journal of Sound and Vibration, 2019, https://doi.org/10.1016/j.jsv.2019.115083.

[42] J. Ching, Y.C. Chen, Transitional Markov chain Monte Carlo method for Bayesian model updating, model class selection, and model averaging, Journal of Engineering Mechanics 133 (7) (2007) 816-832.

[43] F. Tisseur, K. Meerbergen, The quadratic eigenvalue problem, SIAM Review 43 (2) (2001) 235-286.

[44] D. Chronopoulos, Wave steering effects in anisotropic composite structures: Direct calculation of the energy skew angle through a finite element scheme, Ultrasonics 73 (2017) 43-48.

[45] D. Alleyne, P. Cawley, A two-dimensional Fourier transform method for the measurement of propagating multimode signals, The Journal of the Acoustical Society of America 89(3) (1991) 1159-1168.

[46] C. Leon, Time-Frequency Analysis: Theory and Applications. Prentice-Hall, Inc., Upper Saddle River, NJ, USA, 1995.

[47] W.X. Ren, H.B. Chen, Finite element model updating in structural dynamics by using the response surface method, Engineering Structures 32 (8) (2010) 2455-2465.

[48] J.S. Park, Optimal Latin-hypercube designs for computer experiments, Journal of Statistical Planning and Inference 39 (1) (1994) 95-111.

[49] K.Q. Ye, Orthogonal column Latin hypercubes and their application in computer experiments, Journal of the American Statistical Association 93 (444) (1998) 1430–1439.

[50] I. Couckuyt, T. Dhaene, P. Demeester, ooDACE toolbox: a flexible object-oriented Kriging implementation, The Journal of Machine Learning Research 15 (1) (2014) 3183-3186.

[51] I. Couckuyt, T. Dhaene, P. Demeester, ooDACE toolbox, Advances in Engineering Software 49 (3) (2012) 1-13.

[52] M. Balesdent, J. Morio, J. Marzat, Kriging-based adaptive importance sampling algorithms for rare event estimation, Structural Safety 44 (2013) 1-10.

[53] I. Kaymaz, Application of kriging method to structural reliability problems, Structural Safety 27 (2) (2005) 133-151.

[54] H.H. Khodaparast, J.E. Mottershead, K.J. Badcock, Interval model updating with irreducible uncertainty using the Kriging predictor, Mechanical Systems and Signal Processing, 25(4) (2011) 1204-1226.

[55] J.T. Wang, C.J. Wang, J.P. Zhao, Frequency response function-based model updating using Kriging model, Mechanical Systems and Signal Processing, 87 (2017) 218-228.

[56] E. Simoen, C. Papadimitriou, G. Lombaert, On prediction error correlation in Bayesian model updating, Journal of Sound and Vibration 332 (18) (2013) 4136-4152.

[57] E.L. Zhang, P. Feissel, J. Antoni, A comprehensive Bayesian approach for model updating and quantification of modeling errors, Probabilistic Engineering Mechanics 26 (4) (2011) 550-560.

[58] W.J. Yan, L.S. Katafygiotis, Application of transmissibility matrix and random matrix to Bayesian system identification with response measurements only, Smart Materials and Structures 25 (10) (2016) 105017.

[59] D. Lebel, C. Soize, C. Fünfschilling, G. Perrin, Statistical inverse identification for nonlinear train dynamics using a surrogate model in a Bayesian framework, Journal of Sound and Vibration 458 (2019) 158-176.

[60] S.H. Cheung, J.L. Beck, Bayesian model updating using hybrid Monte Carlo simulation with application to structural dynamic models with many uncertain parameters, Journal of Engineering Mechanics 135 (4) (2009) 243-255.

[61] N. Metropolis, A. W. Rosenbluth, M. N. Rosenbluth, A. H. Teller, and E. Teller, J. Chem. Phys. 21, 1087 (1953).

[62] W.K. Hastings, Monte Carlo sampling methods using Markov Chains and their applications, Biometric, 57(1) (1970) 97-109.

[63] W. Betz, I. Papaioannou, D. Straub, Transitional Markov Chain Monte Carlo: Observations and Improvements, ASCE Journal of Engineering Mechanics, 142(5), (2016) 04016016.

[64] S. Wu, P. Angelikopoulos, C. Papadimitriou, P. Koumoutsakos, Bayesian annealed sequential importance sampling: an unbiased version of transitional Markov chain Monte Carlo, ASCE-ASME Journal of Risk and Uncertainty in Engineering Systems, Part B, 4(1) (2018) 011008.

[65] P.E. Hadjidoukas, P. Angelikopoulos, C. Papadimitriou, P. Koumoutsakos, Π4U: A high performance computing framework for Bayesian uncertainty quantification of complex models, Journal of Computational Physics 284 (2015) 1-21.

[66] P. Angelikopoulos, C. Papadimitriou, P. Koumoutsakos, X-TMCMC: Adaptive kriging for Bayesian inverse modeling, Computer Methods in Applied Mechanics and Engineering 289 (2015) 409-428.